Title

Role for Wnt Signaling in Retinal Neuropil Development: Analysis via RNA-Seq and In Vivo Somatic CRISPR Mutagenesis

Journal

Neuron, 98(1)

ISSN

0896-6273

Authors

Sarin, Sumeet
Zuniga-Sanchez, Elizabeth
Kurmangaliyev, Yerbol Z
et al.

Publication Date

2018-04-01

DOI

10.1016/j.neuron.2018.03.004

Peer reviewed

HHS Public Access

Author manuscript

Neuron. Author manuscript; available in PMC 2019 April 04.

Published in final edited form as:

Neuron. 2018 April 04; 98(1): 109–126.e8. doi:10.1016/j.neuron.2018.03.004.

Role for Wnt signaling in retinal neuropil development: analysis via RNAseq and in vivo somatic CRISPR mutagenesis

Sumeet Sarin[1,*], **Elizabeth Zuniga-Sanchez**[2,*], **Yerbol Z Kurmangaliyev**[2], **Henry Cousins**[1], **Mili Patel**[1], **Jeanette Hernandez**[2], **Kelvin X Zhang**[2], **Melanie Samuel**[1], **Marta Morey**[2], **Joshua R Sanes**[1,^], and **S Lawrence Zipursky**[2^]

[1]Center for Brain Science and Department of Molecular and Cellular Biology, Harvard University, Cambridge, MA 02130, USA

[2]Department of Biological Chemistry, HHMI, David Geffen School of Medicine, University of California, Los Angeles, Los Angeles, CA 90095, USA

SUMMARY

Screens for genes that orchestrate neural circuit formation in mammals have been hindered by practical constraints of germ-line mutagenesis. To overcome these limitations, we combined RNAseq with somatic CRISPR mutagenesis to study synapse development in the mouse retina. Here synapses occur between cellular layers, forming two multilayered neuropils. The outer neuropil, the outer plexiform layer (OPL), contains synapses made by rod and cone photoreceptor axons on rod and cone bipolar dendrites, respectively. We used RNAseq to identify selectively expressed genes encoding cell surface and secreted proteins and CRISPR-Cas9 electroporation with cell-specific promoters to assess their roles in OPL development. Among the genes identified in this way are Wnt5a and Wnt5b. They are produced by rod bipolars and activate a non-canonical signaling pathway in rods to regulate early OPL patterning. The approach we use here can be applied to other parts of the brain.

Correspondence: sanesj@mcb.harvard.edu (J.R.S.), lzipursky@mednet.ucla.edu (S.L.Z.).

*These authors contributed equally.

^co-senior authors

2^Lead contact: lzipursky@mednet.ucla.edu

Present addresses: K.X.Z.: Merck Sharp & Dohme Co., Computational Genomics and Informatics, Boston, MA 02210, USA. M.M.: Departament de Genètica, Facultat de Biologia and Institut de Biomedicina (IBUB) de la Universitat de Barcelona, Barcelona 08028, Spain.

M.S.: Program in Developmental Biology, Baylor College of Medicine, Houston, TX 77030, USA, Department of Neuroscience, Huffington Center on Aging, Baylor College of Medicine, Houston, TX 77030, USA.

Author Contributions

S.S., E.Z., J.R.S., and S.L.Z. outlined the project and wrote the manuscript. S.S. and E.Z. performed the *in vivo* experiments and analyzed the data. E.Z. carried out the RNA sequencing, and Y.Z.K. and K.X.Z. analyzed the RNA sequencing data. H.C. performed the *in vitro* experiments, M.P. generated the multiplex vectors, J.H. helped carry out the CRISPR screen, and M.S. developed the protocol for sorting and sequencing fixed cells. M.M. initiated this project in the Zipursky lab and carried out the initial RNA sequencing studies.

Declaration of Ineresets

The authors declare no competing interests.

eTOC blurb

Photoreceptors form synapses on interneurons in the retina. Sarin et al. used RNAseq and somatic CRISPR/Cas9 mutagenesis to seek genes required for this process. They show that Wnt5 produced by bipolar interneurons acts on rod photoreceptors to regulate synapse location.

INTRODUCTION

As the mammalian brain forms, vast numbers of cell types assemble into complex neural circuits. Many genes that regulate neural development have been identified, including key players in steps ranging from neurogenesis to guidance of axons (Kolodkin and Tessier-Lavigne, 2011). In contrast, our understanding of later developmental steps, such as target recognition, formation and maturation of synapses, and formation of laminated neuropil, remains incomplete.

We chose to analyze these steps in the outer retina for several reasons. First, it is one of few regions in the mammalian central nervous system in which all neuronal cell types have been identified and their synaptic connections mapped (Sanes and Zipursky, 2010; Dunn and Wong, 2012; Shekhar et al., 2016; Behrens et al., 2016). Rod and cone photoreceptors populate the outermost layer of the neural retina, the outer nuclear layer (ONL). Their axons terminate in a thin neuropil, the outer plexiform layer (OPL), in which they synapse on interneurons called bipolar and horizontal cells (BCs, HCs), whose somata inhabit an inner nuclear layer (INL) (Figure 1A). Connectivity within the OPL is specific: rods synapse predominantly on rod BCs (RBCs) and axons of HCs in the outer sublamina of the OPL, and cones synapse on cone BCs (CBCs) and HC dendrites in an inner sublamina. Second, the OPL is readily accessible to analysis and manipulation. OPL synapses are large and form postnatally (Olney, 1968; Blanks et al., 1974) and cell type-specific markers are available to monitor pre- and post-synaptic partners. Moreover, outer retinal cells can be transduced by electroporation of neonatal retina *in vivo* (Matsuda and Cepko, 2004; 2007), enabling manipulation of cells that form the OPL before and as it develops. Third, because the synaptic partners are “born” at sites close to their final destinations, and connect by short axons and dendrites, long-distance migration and axon guidance can be ignored.

In considering approaches to finding candidate mediators of late steps in circuit assembly, a key problem is that the number of plausible candidates is large but methods for testing them *in vivo* are cumbersome. Few unbiased screens have been performed in mice (e.g., Bai et al., 2011; Dwyer et al., 2011), owing to factors including relatively long generation time and small litter size. Instead, molecular and histological approaches have been used to complement strategies based on homology to genes implicated in invertebrates. For example, identification of proteins based on their ability to stimulate axon outgrowth or synaptic differentiation *in vitro*, has led to the isolation and characterization of factors regulating circuit development *in vivo* (Serafini et al., 1994; Drescher et al., 1995; Umemori et al., 2004; Christopherson et al., 2005; Linhoff et al., 2009). Alternatively, candidates have been identified on the basis of their spatiotemporal expression during development (Nakamoto et al., 1996; Yamagata et al., 2002). Establishing the function of proteins identified in these ways generally relies on the generation of germ-line knockouts in the

mouse. However, as is the case for unbiased screens, this “reverse genetic” approach is limited by the expense of generating, breeding and testing germ-line mutants. Thus, many key players are likely being missed.

Advances in molecular biology over the past several years led us to consider an alternative strategy. First, RNA sequencing technology (Dong et al., 2016), coupled with methods for cell-type purification (Kay et al., 2012; Siegert et al., 2012), enables a comprehensive approach to identifying genes differentially expressed between specific neuronal types during development. Second, CRISPR-based somatic mutagenesis permits generation of homozygous null mutant neurons in wild-type animals (Holkers et al., 2014; Wang et al., 2014; Swiech et al., 2015; Heidenreich and Zhang, 2016).

Here we combine and extend these methods to facilitate analysis of retinal development in the mouse. We first used a panel of cell type-specific markers to characterize OPL development, discovering a hitherto unrecognized early step in its formation. We then obtained transcriptomes from rods, cones, RBCs and CBCs at key developmental times, identified differentially expressed genes encoding cell surface and secreted proteins, and tested candidates using CRISPR-Cas9 somatic mutagenesis. We found that Wnt5a and 5b are selectively expressed by RBCs and play a role in patterning the OPL. We used cell type-specific manipulation, further mutagenesis and cell culture to show that they act on rods and to dissect their signaling pathway. Together, our results demonstrate a role for non-canonical Wnt signaling in lamina formation and establish a pipeline that can be applied to other regions of the mouse brain.

RESULTS

Development of the OPL

The OPL contains synapses between photoreceptors (rods and cones) in the ONL and interneurons (HCs, RBCs and CBCs) in the INL (Figure 1A). CBCs are further subdivided into 6 types that are inhibited by light (OFF types) and 8 that are excited by light (ON types); (Greene et al., 2016; Shekhar et al., 2016). Except where indicated, however, we treat ON CBCs as a set.

To begin our study, we built on previous work to describe the main cellular events of OPL development (reviewed in Hoon et al., 2014; Zhang et al., 2017). Cones and HCs are born during embryogenesis (E12–E17). Rod development begins in embryogenesis but peaks soon after birth. The first bipolar cells are born just prior to postnatal day (P)0, with peak numbers generated at P3. All ONL and INL neurons are born prior to P10 (Carter-Dawson and LaVail, 1979; Young, 1985). OPL development occurs postnatally in three partially overlapping steps: appearance of the OPL (P0–8) (Figures 1B, S1A), synaptogenesis (P4–13) (Figure 1C), and separation of the rod and cone terminals into discrete sublaminae (P9–21) (Figure 1D). Because retinal differentiation proceeds in a center-to-peripheral wave, times refer to central retina.

Appearance of the OPL—By P0 (Figure S1A), the somata of cones and HCs have segregated, with cones found apically (the future ONL) and HCs basally (the future INL).

However, only a small fraction of the rods and bipolars have formed. The boundary between cell types is incomplete with some mixing of cells between them (discussed further below), and the OPL is not yet present (Figure S1A).

By P2–3 (Figure 1B), cone axons extend into the region of HC somata, and HC processes extend into the region of photoreceptor cell bodies. These neurites are joined by those of recently-born rods, leading to formation of discontinuous neuropil patches at the boundary between the future ONL and INL at P4/5. Over the following few days, gaps between these patches are filled as photoreceptor terminals align and increasing numbers of rods extend axons into the neuropil. HC processes extend laterally along a boundary of developing photoreceptor terminals (Hinds and Hinds, 1979; Huckfeldt et al., 2009). In parallel, thin BC processes retract, and dendrites of BCs invade the nascent OPL (Figure S1C; Morgan et al., 2006). By P8, the OPL forms a continuous layer of axonal and dendritic processes (Figures 1B, S1C″).

Synaptogenesis—Around P3, cone axons bi- or trifurcate forming multiple contacts with individual HC processes (Figure S1B). Typically, one such contact appears bulbous, likely representing an early cone terminal. Electron micrographic studies described HC dendrites invaginating into cone pedicles to form monads at P4, with dyads forming soon thereafter and rod-HC monads appearing by P8 (Olney, 1968; Blanks et al., 1974; Rich et al., 1997). However, the presynaptic cytomatrix protein Bassoon does not appear until P7, suggesting that initial photoreceptor-interneuron contacts are not molecularly specialized.

As BC dendrites form in the OPL (Figure S1C″), they interact with photoreceptor terminals. Cone pedicles form initial contacts with OFF cone bipolar cells at P6 and with ON cone bipolar cells during subsequent days (Sherry et al., 2003). At P7, expression of the pre-synaptic protein Bassoon is widespread, but mGluR6 (an ON BC-specific postsynaptic glutamate receptor apposed to cone terminals) is infrequent (Figures 1C, S1C″). By P13, Bassoon and mGluR6 are clearly visible in rod terminals and RBC dendrites, respectively (Figure 1C).

Sublamination—Initially, synapses formed by rods and cones are intermingled within the OPL (Figure 1D). We used cone arrestin and PSD-95 (a presynaptic marker in rods; Koulen et al., 1998) to label cone and rod terminals, respectively. Near the end of the second postnatal week, rod and cone terminals begin to separate, and RBC dendrites extend further towards the ONL, giving rise to a continuous band of rod spherules above the cone pedicles. Few rod terminals remain positioned within the sublayer of cone terminals. Segregation of terminals into distinct rod and cone sublaminae is complete by P21.

Sorting of rod somata—Surprisingly, the nascent OPL formed not at the interface between rod and BCs, but rather within the nascent ONL: many rods were present between the nascent OPL and bipolar neurons (Figure 2A,B). We identified the cells beneath the OPL as rods using both expression of rhodopsin (Figure 2A), and their rod-specific chromatin pattern (Figure 2B). Rods were not dispersed through the INL, but were arranged in rows between bipolar somata (marked by Chx10, which is expressed exclusively by bipolar cells and Muller glia in postnatal animals) and the OPL (Figure 2B). On average, 4 rows of rod

somata were present in the INL at P4. Subsequently, three events led to a mature OPL: 1) At P5, HCs extended processes that snaked through the INL-population of rods (Figure 2C); 2) By P6, these processes joined the OPL but a few rows of rods remained on the INL side of the OPL (Figure 2C); and 3) By P9, rods and bipolar cells were completely separated by the OPL (Figure 2A,B) as displaced rods disappeared from the INL.

We presume these rods are migrating back across the OPL to the ONL rather than being eliminated by cell death because the ONL increased in size by an equivalent amount during this time (Figure 2D) and occasional rods persisted within the INL (Figure S6F). It is also possible, however, that some ectopic rods are eliminated by apoptosis, or transformed into another cell type.

OPL development is summarized in Figure 2E and 2F.

Transcriptomic analysis of photoreceptor and bipolar neurons

We used RNA sequencing (RNAseq) at three time points to identify candidate regulators of interactions between photoreceptors and BCs: P7, just after the OPL forms and synaptogenesis with BCs begins; P13, as synaptogenesis nears completion and sublamination begins; and P30, when the OPL is mature. We purified cone and rod photoreceptors by FACS using transgene markers: Rho-icre;Ai9 for rods and HRGP (Human Red-Green Protein)-cre;Ai9 for cones. We purified ON BCs, which include ON CBCs plus RBCs using Grm6:GFP (Morgan et al., 2006). As appropriate transgenic lines to separate RBCs from CBCs were not available, we fixed and immunostained cells from Grm6:GFP mice prior to FACS (see Experimental Procedures), allowing us to separate RBCs (GFP +PKC+) and CBCs (GFP+PKC−). PKC is not highly expressed at P7, so we profiled rod and cone bipolars separately only at P13.

We generated two biological replicates for each cell type at each time point and obtained 23–129 million reads per sample (Tables S1,S2). Expression profiles for biological replicates were highly correlated (Figure S2A). The purity of each cell type was confirmed by assessing the expression of previously identified markers. In all cases, appropriate cell-type specific markers were highly enriched and markers of other retinal cell types were present at low levels (Table S3). Approximately 14,000 genes were expressed at least in one cell type at one or more time points.

Differential gene expression analysis—To uncover cell type-specific patterns of gene expression, we performed a pairwise comparison of transcriptomic profiles at each developmental time (Table S4). As expected, many genes were differentially expressed (Figure 3A). At all three time points, 2–3× more genes were enriched >4× in cones compared to rods. Similarly, 2× more genes were enriched in CBCs compared to RBCs at P13. Differences between photoreceptors and ON BCs were more striking, consistent with the greater similarity of cones and rods to each other than to BCs.

We also compared each cell type at different developmental times (Table S4). Gene expression differences across times varied over three orders of magnitude (Figure 3A). Marked differences in gene expression were seen for ON BCs whereas cones were more

stable; rods were intermediate between those in ON BCs and cones. These differences, may partly reflect relative birth dates; cones are generated prenatally, whereas many rods and BCs are newborn at P7 (Young, 1985). Another possibility, discussed below, is that the differences reflect cell type diversity within each class.

Transcription factors, channels, receptors, and transporters—Transcription factors, channels, receptors, and transporters were differentially expressed among the different cell types (Figure S3). A few of these had been described previously (Table S3) but the majority are novel.

Cell surface and secreted proteins—Neuronal interactions are generally mediated by cell surface and secreted proteins (CSP) so we focused on genes that encode them. First, we evaluated enrichment of cell surface proteins among the differentially expressed (DE) genes by determining the fraction of genes associated with the gene ontology category (GO-term) “plasma membrane” (GO:0005886). Of the 13,812 genes expressed in this dataset, 11% were associated with this category (Table S5). More plasma membrane genes were differentially expressed between rods and cones at P7 and P13, and between RBCs and CBCs at P13 than expected by chance (Fisher’s exact test, $p<0.05$). Because no GO term is ideally suited to capture all CSPs, we also generated a list of 793 CSPs from all DE genes (Figure 3B and STAR methods), allowing us to identify secreted and plasma membrane proteins not covered by the GO term.

To analyze candidate mediators of interactions between photoreceptors and BCs, we focused on P13. The comparison between rods and cones yielded 41 CSPs enriched in rods and 156 in cones. The comparison between RBCs and CBCs identified 141 genes enriched in CBCs and 55 in RBCs (Figure 3C). These proteins include members of several groups including cadherin and Immunoglobulin (Ig)-superfamily proteins (Figure 3D). Some members of these families have previously been shown to mediate interactions between developing neurites (Kolodkin and Tessier-Lavigne, 2011; de Wit and Ghosh, 2016).

The availability of single cell sequencing data from RBCs (a single type) and the eight ON CBC types allowed us to explore the discrepancy between the enrichment of DE genes in RBCs and ON CBCs. We compared the expression of genes encoding CSPs identified in our study with single cell profiling data (Figures 3E, S2B; for a broader comparison of methods see Shekhar et al., 2016). This analysis showed that each ON CBC type expressed on average 70% more DE CSPs than RBCs. Thus, the increase in the diversity of CSPs we observed in CBCs reflects both the number of different ON CBCs and the increased number of CSPs expressed in each CBC type.

CRISPR-based assay to mutate genes in the outer retina

We next developed a method to assay the function of differentially expressed genes using CRISPR-Cas9 to mutate target genes in somatic cells (Swiech et al., 2015). Methods have been developed to introduce genes into neonatal retina, prior to OPL formation, using electroporation and viral vectors (Matsuda and Cepko, 2004; Duan et al., 2014; Wang et al., 2014). We used electroporation due to the relative ease of constructing vectors, and the shortened latency of expression from plasmids compared to viral vectors. We designed at

least two 20bp guide RNAs per gene, using criteria detailed in STAR methods, and used *S. pyogenes* Cas9.

Perturbing gene function in rods—Electroporation of neonatal retina transduces dividing cells efficiently, but postmitotic cells poorly (Matsuda and Cepko, 2004; 2007). This method therefore transduces precursors to rods, BCs, and Muller glial cells, but neither HCs nor cones. To develop an assay, we first targeted Nrl, a transcription factor that is selectively expressed in rods and represses cone fate (Mears et al., 2001). In Nrl mutants, rods are converted into cone-like cells (referred to as "cods"), including expression of the cone opsin, S-opsin, which is readily assayed by immunostaining.

We compared CRISPR-Cas9 targeted Nrl gene inactivation to an shRNA and a dominant negative construct (Figure 4A–C). In each case, electroporation was performed at P0 and retinas were assayed at P21. The CRISPR-Cas9 strategy was most successful. Both of the Nrl sgRNAs tested (termed Nrl^{CRISPR}) led to S-opsin expression in 40–50% of GFP-positive cells in the ONL. By contrast, the penetrance of the phenotypes seen with the Nrl shRNAs and the dominant negative construct was approximately 30% and 10%, respectively (Figure 4C). No GFP-positive cells expressed S-opsin in retinas electroporated with a control plasmid. Because one copy of Nrl is sufficient to repress the cone fate, these data indicate that knockout of both alleles in electroporated cells is highly efficient. Electroporating a single plasmid encoding GFP, the sgRNA and Cas9 (Ran et al., 2013) increased the penetrance (S-opsin positive cells/GFP-positive cells) further, to ~90% (Figure 4C). We detected S-opsin in GFP-positive cells by P6, the earliest time examined. Thus, homozygous mutagenesis and its consequences can be assayed within 5 days of introducing reagents. Based on these results and those of others (Shalem et al., 2014), we used CRISPR-Cas9 in subsequent studies.

To assess the utility of the CRISPR-Cas9 method for manipulating rods, we targeted *Psd-95, Bassoon, Cadm1, and Elfn1*. PSD-95 and Bassoon are components of rod terminals. In these and other cases described below, we chose sgRNAs to mutate genes at or near the 5′ end of the coding sequence to maximize the chance of generating null alleles. In both $Bassoon^{CRISPR}$ and $Psd\text{-}95^{CRISPR}$, protein expression was eliminated in many rod terminals (Figure S4A). Furthermore, HC and BC sprouting was observed in $Bassoon^{CRISPR}$ (Figure 4G), as previously reported in a germline mutant allele (Dick et al., 2003). Elfn1 is expressed in membranes of rod terminals. In germ-line mutants, glutamate receptors (mGluR6) fail to cluster on dendrites of RBCs (Cao et al., 2015). A similar loss was apparent in $Elfn1^{CRISPR}$ (Figure 4D and S4B). *Cadm1* is a cell adhesion molecule selectively expressed on rods. In $Cadm1^{CRISPR}$ retinas, HC processes sprouted as previously described in *Cadm1* germline mutants (Ribic et al., 2014). By contrast to Bassoon mutants, however, RBC or CBC sprouting was not seen in either germline or $Cadm1^{CRISPR}$ alleles (Figure 4G). Thus, CRISPR-based mutagenesis effectively knocks down proteins localized to synapses, is effective in generating specific OPL wiring phenotypes and can generate non-autonomous phenotypes.

Perturbing gene function in bipolar cells—To assess CRISPR-Cas9 mutagenesis in bipolar cells we targeted the RBC and CBC markers, *Prkca (PKC)* and *Secretagogin (Scgn)*,

respectively (Haverkamp et al., 2000; Puthussery et al., 2010), and used the mGluR6 promoter to selectively express Cas9 in ON BCs. The number of PKC-positive GFP-labeled BCs was reduced by 33% in response to *PKC*^{CRISPR}, and the number or Scgn-positive GFP-labeled BCs was reduced by 59% in response to *Scgn*^{CRISPR} compared to controls (Figures 3E, S4C,D). *PKC*^{CRISPR} had no effect on Scgn expression and *Scgn*^{CRISPR} had no effect on PKC expression.

Perturbing gene function in cone-like cells ("cods")—As noted above, cones are not transduced by electroporation at P0. To assay genes selectively expressed in cones, we generated a single plasmid to simultaneously mutate both Nrl (converting rods into "cods"; Figure 4B) and a cone-specific gene. Consistent with results from *Nrl* mutant mice, the position and morphology of *Nrl*^{CRISPR}-generated cods were similar to those of cones (Figure 4B). The "cod" outer segments exhibited a cone-like structure and "cod" cell bodies occupied the outer portion of the ONL characteristic of cones (Figures 4B, S4E). Furthermore, cod axon terminals were similar to those of cones. They were larger than rod terminals, stained by the lectin peanut agglutinin (PNA), and resided within the cone terminal sub-lamina of the OPL (Figures 4B, S4E). In addition, the distribution of Cacna1s, a Calcium channel localized to synapses, was ovoid, as in cones, rather than punctate, as in rods (Figures 4B). Finally, gene expression profiles for cods reported by Kim et al. (2016) were more similar to cone than rod profiles generated in our study (Figure S4F).

To assess the efficacy of this multiplex strategy, we targeted *Psd-95* and *Bassoon* (Figures 4F, S4G). In each case, we compared use of two separate plasmids (one encoding Nrl sgRNA and one encoding the Psd-95 or Bassoon sgRNA) with a single multiplex vector encoding both sgRNAs. In both cases, the sgRNA decreased expression of the targeted protein to undetectable levels in many cods (S-opsin-positive), and the fraction of cods mutated was higher with the multiplex plasmid (58% *Nrl/Psd-95* double KO; 80% *Nrl/Bassoon* double KO) than with the two-plasmids separately (40% and 27%, Figures 4F, S4G).

In summary, CRISPR-based electroporation reliably induced homozygous mutations in rods, bipolar cells, and cones (i.e. cods).

CRISPR-based mutagenesis of candidate mediators of OPL development

We used CRISPR-based screening to assess the function of differentially expressed cell surface proteins in rods, cones and bipolars. To identify candidates, we first used stringent criteria for differentially expressed genes at FDR 5% with a minimum fold change cut-off >4. Second, from this set, we selected genes encoding cell surface or secreted proteins. Third, among these, we prioritized gene families known to be involved in axon guidance and synapse formation (Figure 3D).

Retinas were electroporated at P0 and phenotypes were scored at P21. In our pilot screen, knock-outs of 8 of 30 genes tested led to detectable outer retinal phenotypes (Table S6). Three phenotypes were, to our knowledge, novel. In *Gpc-2*^{CRISPR} mutants, inactivating a glypican, rod terminals were enlarged by ~50% while other aspects of cell morphology appeared unaffected (Figure 5A). *Wisp1*^{CRISPR} inactivates a secreted protein induced by

Wnt signaling, resulting in rod terminals being positioned more apically within the OPL (Figure 5B). Thus, these genes may be involved in maturation and positioning of rod terminals, respectively. Simultaneous loss of *Wnt5a/5b* gave rise to a supernumerary OPL (discussed further below).

In the five other cases, CRISPR knockouts led to sprouting of interneuronal processes into the ONL. They were: Bassoon (Dick et al., 2003), in rods and cones; Syndig1L/Capucin, a paralog of Syndig1, which binds AMPA receptors (Kalashnikova et al., 2010), in cones; Cadm1 (Ribic et al., 2014), in rods; Tmem108/Retrolinkin, an endosomal trafficking membrane protein (Fu et al., 2011), in rods; and Ptprz1, a protein tyrosine phosphatase receptor (Maurel et al., 1994), in bipolar cells. Interneuronal sprouting has been observed in germ-line *Cacna1f* (Chang et al., 2006), *Ngl-2* (Soto et al., 2013), *Lkb1* (Samuel et al., 2014) and *PlexA4* (Matsuoka et al., 2012) mutants and in aging mouse and human retina (Samuel et al., 2014). Sprouting may be a common response to a variety of perturbations of photoreceptors or interneurons. However, differences between these phenotypes suggest some specificity: (1) in $Bassoon^{CRISPR}$ (as well as in *Cacnca1* and *Lkb1*) retinas both HCs and BCs sprouted (Figure 4G); (2) in Nrl^{CRISPR} $Syndig1L^{CRISPR}$, $Tmem108^{CRISPR}$, $Cadm1^{CRISPR}$, and $Ptprz1^{CRISPR}$ only HC sprouting was seen (Figures 4G, 5C,D, S5); and (3) in $Ptprz1^{CRISPR}$ retinas, PSD-95-rich puncta, likely reflecting ectopic rod terminals, were seen within the ONL (Figure 5D).

Wnt5 is required for OPL development

We initially chose Wnt5a and Wnt5b for analysis because they were selectively expressed by RBCs (Figures 6A, S5D), unique among 19 Wnt ligands. As both Wnt5a and 5b were reported to interact with the same receptors (Keeble et al., 2006; Lin et al., 2010; Yu et al., 2012), we used the multiplex vector to knockout both simultaneously using two separate sets of sgRNAs. Both sgRNAs pairs induced a partially duplicated neuropil as did each Wnt5 sgRNA separately (Figure 6B, Table S6). The ectopic OPL was separated from the normal OPL by ~7 μm. One to three layers of somata were present between the two laminae. Using a panel of markers, we found that most if not all, of the intercalated somata were rods (Figure S6A–C).

We used additional markers to assess the composition of the doubled OPL. Both OPLs in doubled regions comprised processes of rods, cones, RBCs, CBCs and HCs (Figure 6C). Furthermore, the apposition between pre- and post-synaptic markers, as assessed using PSD-95, Bassoon and mGluR6, appeared normal within the ectopic OPL (Figure 6D), suggesting the presence of synapses between rod terminals and RBC dendrites. Thus, loss of Wnt5 does not affect subcellular localization of synaptic markers, but rather placement of the synapses.

We also inactivated Dishevelled (Dvl), an intracellular mediator of many Wnt-dependent signaling pathways. One of three mammalian Dvl paralogs, Dvl1, is expressed at highest levels in all outer retinal cells (Figures 6A, S5D). Mutation of *Dvl1* resulted in an ectopic OPL (Figure 6B), confirming that the ectopic OPL phenotype is due to disruption of the Wnt pathway.

Wnt5 acts through a Ryk-dependent pathway

Wnts act through canonical (beta catenin-dependent) and non-canonical (beta catenin-independent) pathways, with all canonical and most non-canonical signaling requiring Dvl. To determine which pathway regulates early OPL formation, we assayed Wnt receptors expressed in rods or BCs (Figure 6A). These included Lrp6 for the canonical pathway and the atypical tyrosine kinase Ryk for the non-canonical pathway, (He et al., 1997). Removal of *Lrp6* did not lead to an ectopic neuropil (Figure 7A). Likewise, no alterations in the OPL were observed following removal of canonical Wnt-enhancers *Rspo2* or *Lgr4* or overexpression of *Dkk1*, an inhibitor of the canonical pathway (Figure S5A). By contrast, removal of *Ryk*, using two different sgRNAs, resulted in an ectopic OPL similar to that observed with $Wnt5a/5b^{\mathrm{CRISPR}}$ (Figure 7A). The ectopic OPL generated by Ryk^{CRISPR}, like that generated by $Wnt5a/5b^{CRISPR}$, included processes of rods, cones, RBCs, CBCs and HCs (Figure 7B). These results suggest that Wnt5a/5b signal through the Ryk receptor.

Ryk often acts with co-receptors, including the Fzd- and Vangl-type receptors (Lu et al., 2004; Kim et al., 2008; Andre et al., 2012). Fzd4 and Fzd5, but not Vangl-family proteins, are expressed in the developing outer retina (Table S2;Figure 6A). Neither $Fzd4^{\mathrm{CRISPR}}$ nor $Fzd5^{\mathrm{CRISPR}}$ induced phenotypes when knocked out individually but knocking them both out resulted in an ectopic OPL (Figure 7A).

We next assessed when Wnt5/Ryk signaling from RBCs to rods is required for OPL development. We observed ectopic nascent OPLs surrounding one or two rows of rod somata in $Wnt5a/Wnt5b^{\mathrm{CRISPR}}$ and Ryk^{CRISPR} as early as P6, which is the earliest we can visualize PSD-95 expressing rod terminals (Figure 7C). Cone terminals were present in both neuropils by P6 (Figure S6C). Thus, Wnt/Ryk signaling is required for the development rather than the maintenance of the OPL.

Together, these data support a model in which Fzd4, Fzd5 and Ryk act in combination to regulate OPL development by transducing the Wnt5a/Wnt5b signal via a Dvl-dependent non-canonical signaling pathway.

Rods receive the Wnt5 signal

To determine which cells respond to Wnt5, we targeted Ryk^{CRISPR} and Dvl^{CRISPR} to rods or ON BCs using Rhodopsin and mGluR6 promoters, respectively (see STAR methods). In both cases, rod-restricted expression led to an ectopic neuropil; no phenotype was observed by knocking out Ryk or Dvl in BCs (Figure 7D). Likewise, mutating Fzd10 (the most abundant cone Fzd) or Dvl1 in cods (Nrl^{CRISPR} $Fzd10^{\mathrm{CRISPR}}$ or Nrl^{CRISPR} $Dvl1^{\mathrm{CRISPR}}$) led to modest levels of HC sprouting but not to formation of a duplicated OPL (Figure S5B–D).

Although Wnt appears to act on rods, our results did not distinguish between a direct effect and relay mechanisms in which RBC-derived Wnt5 acts on another cell that in turn affects rods. To distinguish these alternatives, we developed a culture system for photoreceptors. Retinas were dissociated at P3 and cultured for 3 days in defined medium. Rods, identified by immunostaining for Rhodopsin, comprised ~70% of the cells in these cultures, corresponding to their prevalence in whole retina (Jeon et al., 1998). In some experiments,

we enriched rods to >90% by purifying them on immunomagnetic beads coated with antibodies to CD73, a rod-specific marker.

In both cases, rods formed short neurites under control conditions, and neurite length approximately doubled when medium was supplemented with Wnt5a or Wnt5b (Figure S7). Wnt5a and 5b together did not further enhance neurite outgrowth, suggesting that they act through the same receptor (Figure 7E,F, S7G). Neurite outgrowth of rod cultures was unaffected by Wnt3a (Figure S7A) an inducer of the beta-catenin dependent/canonical pathway (Yue et al., 2008).

To confirm that Wnt5 was acting through Ryk, we cultured rods that had been electroporated with *Ryk*^{CRISPR} *in vivo*, and stained them with an antibody to Ryk. Among transfected rhodopsin-positive cells, >60% showed partial or complete knockdown of Ryk protein (Figures S7B, S7C), demonstrating the efficacy of *Ryk*^{CRISPR}. Neurites of rods lacking Ryk were non-responsive to Wnt5a or Wnt5b (Figures 7E, S7D).

We also used the culture system to assess effects of Wnt5 on cones. When cultured in isolation (following purification with anti-CD133; see STAR methods), cones survived, but failed to extend processes in the absence or presence of Wnt5. In unpurified cultures, cones did extend processes. Whereas Wnt5 increased neurite length of rods in these cultures, it had no detectable effect on cone neurites (Figures S7E,F).

These data support a model in which Wnt5a/5b produced by rod bipolars acts directly on rods to pattern the OPL.

Germline mutations phenocopy CRISPR-induced somatic mutations

We crossed conditional *Ryk* germline mutants (Hollis et al., 2016) to the Rho-icre line described above to generate mice in which *Ryk* was selectively deleted from rods. (Constitutive Ryk deleted-mice die shortly after birth; Halford et al., 2000). We observed patches of supernumerary OPL (Figure 7G), similar to those observed in *Ryk*^{CRISPR} electroporated patches in both hetereozygous (n=2/4) and null (n=1/2) mutants but not in wild types (n=0/3). These results validate two important aspects of our CRISPR mutagenesis method. The phenotype of the CRISPR mutants was concordant with that of “gold standard” germ line mutant and the cellular site of action of a gene (rods for Ryk) inferred from the CRISPR mutant was concordant with that inferred from cre-dependent deletion of a germline conditional mutant.

Surprisingly, the phenotype observed in the *Ryk* germ-line mutant was not more penetrant than that observed in the CRISPR mutant. This “patchiness” might reflect a genuine biological phenomenon or incomplete deletion of floxed Ryk from photoreceptors. To distinguish between these alternatives, we analyzed a germ-line constitutive *Dvl1* mutant (Lijam et al., 1997). Three of four mutants displayed a supernumerary OPL akin to our *Dvl1*^{CRISPR} electroporated patches, while two heterozygous animals appeared normal (Figure 7G,H). However, the expressivity remained low; each retina displayed a single duplicated event, ~200 μm across. The low phenotypic incidence indicates that the positioning of the OPL is tightly regulated, likely with redundant mechanisms.

DISCUSSION

Understand the mechanisms by which neurites recognize one another and form an organized neuropil is difficult owing to the diversity of neuronal types and the extraordinary specificity of synaptic connections among them. The recent development of cell-specific markers for purifying cells (Kay et al., 2012), RNA sequencing methods for identifying the genes they express (Siegert et al., 2012), and CRISPR-based somatic mutagenesis to assess their function (Holkers et al., 2014; Wang et al., 2014; Swiech et al., 2015; Heidenreich and Zhang, 2016), prompted us to adapt these methods to understanding wiring in the mammalian brain.

We focused on the outer retina, not only because of its accessibility and relative simplicity, but also because photoreceptors exhibit at least three forms of synaptic specificity in the OPL: cellular (rods and cones synapse on RBCs and CBCs, respectively); subcellular (rods synapse on HC axons, and cones on their dendrites); and laminar (rod and cone terminals are confined to outer and inner strata, respectively, within the OPL). Although specificity is not absolute (Pang et al., 2010), the relatively simple structure and largely binary nature of synaptic choices in the OPL make it an attractive region for mechanistic analysis of neuropil assembly.

Using RNA sequencing, we identified many cell surface and secreted proteins selectively expressed by rods, cones, RBCs or CBCs. We then demonstrated that inactivation of gene function in somatic cells via CRISPR provides a robust method for assessing the function of these proteins. Following an initial screen, we focused on Wnt signaling, demonstrating that OPL formation is regulated by Wnt5a/5b from rod bipolars signaling to rods via a Ryk/Fzd4/Fzd5/Dvl pathway.

Non-canonical Wnt signaling from RBCs to rods regulates OPL development

CRISPR-mediated mutagenesis of Wnt5a and Wnt5b led to segments of duplicated OPL. To pinpoint the signaling pathways and cells through which Wnt5a/5b act, we used our RNAseq data to identify putative Wnt receptors and signal transduction components expressed in the outer retina. We found that Wnts act through a non-canonical pathway using Ryk, Fzd4 and Fzd5 as receptors. Finally, we used cell type-specific promoters driving Cas9 to identify rods as the receiving cells. Together, these results show that Wnt5a/5b produced by RBCs is detected by Ryk/Fzd4/5 co-receptors and Dvl in rods, and functions to organize developing neurites into a single neuropil (Figure 7I).

Although CRISPR-based somatic mutations of five Wnt-related genes (Ryk, Dvl1, Wnt5a, Wnt5b, Wnt5a/5b, Fzd4/5) all led to a similar duplicated OPL, the penetrance of the phenotype was low in all cases. We wondered whether this reflected limited ability to mutate genes –for example generation of hypomorphs or heterozygotes rather than homozygous null cells. To test this idea, we analyzed germline mutants of Dvl1 and Ryk. Animals of both genetic backgrounds phenocopied their CRISPR counterparts with similarly low penetrance. This low penetrance could be due to several factors, including redundancy, presence of genetic modifiers or genetic compensation. Importantly, it is not due to inherent limitations in somatic CRISPR mutagenesis.

Our results add to the many roles that Wnts and Ryk play in neural development in worms, flies and mice (Klassen and Shen, 2007; Dickins and Salinas, 2013; Fradkin et al., 2010; Fujimura, 2016). Thus, Wnts, like other major developmental signals (e.g. Hedgehog, FGF and BMPs), act in multiple contexts.

How does Wnt5a/5b regulate OPL development?

The cellular mechanisms by which disruption of Wnt signaling from RBCs to rods affects OPL development remain unclear. We suggest three alternative models. First, consistent with our in vitro experiments, Wnt5 may act directly upon rod terminals to promote growth towards the OPL. In its absence, rod terminals would fail to extend to the definitive OPL, generating an ectopic layer to which processes of cones, BCs and HCs would be recruited.

Second, consistent with roles of Wnt in presynaptic differentiation and maturation in cerebellum (Hall et al., 2000), Wnt signaling could stabilize interactions between rod terminals and their targets. Failure to stably adhere may result in retraction. In this scenario, as in the first, misplaced terminals within the ONL would then nucleate a separate OPL.

A third model is suggested by the previously unappreciated aspect of early retinal development we uncovered in studies of wild type animals. The conventional view of OPL assembly is that it is preceded by formation of a boundary between two cell classes, photoreceptors (rods and cones) within the ONL, and interneurons (BCs and HCs) within the INL. We were surprised to find that at early stages, rod somata are present on both sides of the OPL. That is, the OPL initially forms within the ONL. This pattern has not, to our knowledge, been discussed, but is apparent in published images (Katoh et al., 2010; Brzezinski et al., 2013). As development proceeds, these misplaced rods disappear by migrating into the ONL, converting to bipolar neurons or dying. The ONL expands as the INL contracts, suggesting that the misplaced neurons migrate into the ONL. In this view, Wnt signaling from underlying RBCs could repel or “push” the ectopic rods into the ONL, consistent with well-documented abilities of Wnts to repel axons (Liu et al., 2005; Keeble et al., 2006) and promote directional translocation of cells (Witze et al., 2008). In the absence of Wnt signaling, the ectopic rods persist and, along with HC axons, nucleate a patch of doubled OPL. It is also possible, however, that Wnts affect the fate of postmitotic cells, which are known to transiently retain the capacity to differentiate into either rods or bipolars (Brzezinski et al., 2013).

In principle, live imaging would allow us to discriminate among these models, but the low penetrance of the phenotype makes this infeasible.

Advantages of pathway analysis using somatic CRISPR mutagenesis

Many strategies have been used to elucidate cellular and molecular mechanisms underlying circuit assembly in mammals, but all have limitations. Unbiased loss-of-function mutagenesis screens in mice are expensive and laborious. Few culture systems are available that exhibit synaptic specificity or form organized neuropil. The number of candidates that can be tested by germ-ling knock-out methods is limited. By combining RNAseq and somatic CRISPR mutagenesis, we are able to circumvent some of these limitations. RNAseq enables generation of fairly comprehensive lists of candidate mediators of intercellular

interactions. CRISPR mutagenesis via electroporation as we have done here or with viral vectors (Holkers et al., 2014) enables testing a relatively large number of candidates in vivo.

Our studies of Wnt signaling illustrate multiple strengths of somatic CRISPR mutagenesis to study postnatal retinal development. First, once we had demonstrated a phenotype for Wnt5, we were able to analyze its signaling mechanisms rather quickly by identifying signal transduction components expressed in the outer retina and mutating 8 of them. Similar tests with germ-line methods would have been considerably slower and more expensive.

Second, somatic methods allow interference in specific cells at specified times in development. For example, germ-line deletion of Ryk leads to lethality, so use of conditional mutants and cell-type specific drivers would have been needed to assess its involvement and demonstrate the cells in which it acts. Similarly, as Wnt signaling acts at both early and late stages of retinal development (Fujimura, 2016), additional steps would have been necessary to disentangle embryonic and postnatal roles.

Third, multiplex vectors permit mutagenesis of multiple genes simultaneously. For instance, whereas deletion of neither Fzd4 nor Fzd5 alone had a detectable effect, the double mutant exhibited a duplicated OPL. Such redundancy (or compensation) is common in mammalian systems and represents a considerable impediment to genetic analysis. Vectors are available that allow for the simultaneous removal of up to 7 genes by multiplexing (Sakuma et al., 2014).

Finally, although we focused on OPL formation, the method can be used to analyze multiple steps in neural development, and can likely be extended to analysis of neural function in adults.

In conclusion, combining RNAseq to identify candidates with somatic CRISPR mutagenesis to test them provides an effective way to analyze mammalian circuit assembly in vivo. Recent results indicate that this method can be applied to many brain regions (Swiech et al., 2015; Shinmyo et al., 2016; Uezu et al., 2016). Improvements in CRISPR technology, RNAseq, and automated imaging, will further enhance the power of this approach, extending the range of problems and regions to which it can be applied.

STAR Methods

CONTACT FOR REAGENT AND RESOURCE SHARING

Further information and requests for reagents may be directed to, and will be fulfilled by the Lead Contact S. Lawrence Zipursky.

EXPERIMENTAL MODEL AND SUBJECT DETAILS

Animals—Mice were handled and tissue obtained following protocols approved by the Harvard University Standing Committee on the Use of Animals in Research and Teaching and the Chancellor’s Animal Research Committee (ARC) at UCLA. CD1 mice used for electroporations were obtained from Charles River (Cambridge). P0 indicates the day pups were born. Unless otherwise indicated, pups were electroporated at P0–1 and sacrificed at

P21. Males and females were both used for RNA sequencing and electroporation experiments.

The following mouse lines were used in this study:

1. Tg(B6;SJL-Pde6b+ Tg(Rho-icre)1Ck/Boc) to isolate rods (Li et al., 2005) and Tg(OPN1LW-cre)#Yzl) to isolate cones (Le et al., 2004) were kindly provided by Dr. XianJie Yang at UCLA.
2. Tg((Grm6-EGFP)5Var) for sorting bipolar cells (Morgan et al., 2006) were generously provided by Dr. Rachel Wong at University of Washington.
3. Conditional deletion of Ryk crossed into Ai14 trangenic animals ($Ryk^{flox/flox}$) were kindly provided by Dr. Yimin Zou at UCSD.
4. Germline knockout of Dvl1 were kindly provided by Anthony Wynshaw-Boris at Case Western Reserve University.

METHOD DETAILS

Sorting Cell Types and Library Construction

LIVE sample preparation (rods, cones, ON bipolars): Eyes were enucleated from 3 animals and their retinas were dissected. Retinal tissue was collected in HBSS, calcium, magnesium with 10% Fetal Bovine Serum (referred as HBSS+) media. Tissue was spun at 1000rpm for 30 secs and washed twice with HBSS, no calcium, no magnesium (referred as HBSS−) media. Media was replaced with HBSS− containing 100 units/mL of Papain and 0.18 Wu/mL of Liberase TM. Tissue was incubated at 37°C for 15 min in a microfuge shaker at 1,000 rpm. Cells were mechanically dissociated by pipetting up and down with a P1000 tip at 5 and 10 min into this incubation. At 15 min, digestion was inactivated by addition of HBSS+ media and the sample was treated with 50 ug/mL of DNAse. Further dissociation was performed by passing the sample through a 21G 1 ½-gauge needle. The single cell suspension was then passed through a 70 μm filter. To concentrate the cells, the sample was spun down at 1,600 rpm for 8 min at 4°C. After decanting the supernatant, cells were re-suspended in ~300 μl of HBSS+ media and sorted in a BD FACSAria II.

To prevent rod contamination in the cone sort, rods were first sorted and a “rod gate” was created based on cell size (FSC) and granularity (SSC). During the cone sort, cells that fell in this rod gate were excluded.

FIXED sample preparation (RBC and CBC): Dissociation was performed as mentioned above. Cells were then spun at 350 rcf at 4°C for 10 mins and resuspended in 250 uL of MEM, no glutamine with 4% Bovine Serum Albumin media (referred as MEM-B). Then 1 mL of Paxgene Tissue fix was added to the cell suspension and incubated at room temperature for 1 min. The sample was spun at 2,500 rcf for 2 mins and fixative was replaced with 1 mL of Paxgene Tissue stabilizer and incubated for 1 min at room temperature. Cells were spun again and stabilizer was replaced with 1 mL of PBS containing RNAsin Plus RNase inhibitor (1:100). Sample was washed one more time with the PBS containing RNAsin. Cells were then incubated with MEM-B containing 10% saponin and

RNAsin (1:50) referred as MEM-BSR while gently shaking at 500 rpm for 5 mins at 4°C. Solution was then replaced with a 1:750 dilution of PKC antibody in MEM-BSR and cells were incubated for 30 mins while gently shaking at 4°C. After incubation, cells were rinsed twice with MEM-BSR. Solution was replaced with a 1:500 dilution of Goat anti-Mouse 647 antibody in MEM-BSR. Cells were incubated with secondary antibody for 30 mins while gently shaking at 4°C and then rinsed twice with MEM-BSR. Cells were concentrated in a final volume of 300 uL of MEM-B containing RNAsin (1:50) and sorted in a BD FACSAria II.

cDNA library construction: Cells were collected in Extraction buffer from the Arcturus PicoPure RNA Isolation kit after sorting and RNA was isolated using the same kit. mRNA was amplified in a linear fashion using the Arcuturus RiboAmp HS PLUS kit. cDNA libraries were generated using the TruSeq RNA Library Prep kit v2 and analyzed by 50 bp paired-end sequencing on an Illumina HiSeq 2000 platform.

RNA sequencing analysis—RNA sequencing reads were aligned to the reference mouse genome (GRCm38/mm10) using STAR (Dobin et al., 2013). Raw gene expression counts were calculated for annotated protein coding and lncRNA genes (Ensembl v. 86). Gene counts were generated for uniquely mapped reads using STAR. We excluded genes with low levels of expression. In total, 13,812 genes with expression level of CPM (counts-per-million) > 4 in at least one sample were kept for further analysis. Raw gene counts were then normalized using edgeR (TMM method, Robinson et al. 2010) and used for calculation of gene expression values as logCPM (log2-counts-per-million). Spearman correlation coefficients were calculated between each pair of samples using R (3.3.2)

Differential gene expression analysis: Differential gene expression analysis was performed using edgeR (Robinson et al. 2010) as described in (Chen et al. 2016). P-values were corrected for multiple tests using Benjamini-Hochberg false discovery rate (FDR) method implemented in R (3.3.2). We identified DE genes at FDR 5% with a minimum fold change cut-off greater than 4 (log2-fold-change or logFC > 2).

Annotation of cell surface and secreted proteins: We selected DE genes with an annotated signal peptide and/or one or more transmembrane domains. We then manually excluded known intracellular membrane-bound proteins (e.g. Golgi proteins). In this way, we compiled a list of 794 DE genes encoding putative CSPs, including plasma membrane-bound and secreted molecules (Figure 3B). First, we calculated enrichment of cell surface proteins (CSPs) among the lists of differentially expressed genes using Gene Ontology (GO, Ashburner et al. 2000). We defined genes associated with the broad GO category “plasma membrane” (GO:0005886) and its offspring terms. We used Fisher’s exact test to estimate the significance of enrichment of cell surface and secreted proteins (CSPs) among differentially expressed (DE) genes compared to the background set of genes used in analysis (13812 genes). Next, we performed a manual curation of putative CSPs among all identified DE genes. We selected DE genes with an annotated signal peptide and/or one or more transmembrane domains. We then manually excluded known intracellular membrane-bound proteins (e.g. Golgi proteins).

Comparison with published sequencing data: We compared expression profiles of differentially expressed CSPs between RBCs and CBCs to published single cell profiling of different subtypes of bipolar cells (Shekhar et al. 2016). Tables with normalized single-cell expression profiles and cell type identities from (Shekhar et al. 2016) were downloaded from Single-Cell RNA-Seq Portal (https://portals.broadinstitute.org/single_cell/). For each analyzed gene we calculated the percentage of cells in each bipolar subtype with expression value more than 0. Figure 3E shows the number of RBC- or CBC-enriched CSPs that were also detected by DropSeq in at least 5% of cells.

We also compared results of our analysis with recently published RNA sequencing data from wild-type rods (Nrl WT) and Nrl knockout (Nrl KO) mice (Kim et al. 2016). Normalized transcript expression profiles were downloaded from RetSeq Database (https://retseq.nei.nih.gov/). Expression values (FPKM) for different isoforms of same genes were summed together, and mean gene expression values were calculated for each cell type (i.e. Nrl WT or Nrl KO) at P14. Next, we calculated log2-fold-change in gene expressions between Nrl WT and Nrl KO as $\log FC_{WT/Nrl\text{-}KO} = \log_2(FPKM_{WT}) - \log_2(FPKM_{Nrl\text{-}KO})$. Similarly, we calculated log2-fold-change in gene expression between Rods and Cones at P13 in our dataset as $\log FC_{Rods/Cones} = \log_2(CPM_{Rods}) - \log_2(CPM_{Cones})$. In particular, we focused on comparison of $\log FC_{Rods/Cones}$ to $\log FC_{WT/Nrl\text{-}KO}$ values for CSPs differentially expressed between rods and cones (see Figure S4 F).

Plasmid Construction

Plasmids: For single sgRNA/Cas9 expression we used either px458 (Ran et al., 2013) or px330 (Cong et al., 2013). Guide RNAs (sgRNAs) are cloned downstream of the U6 RNA Polymerase III promoter. Three vectors were used, in which Cas9 and GFP were expressed either separately (px330) or together (px458), or two sgRNAs were expressed simultaneously (px458 multi). px458 contains coding sequences for SpCas9 and GFP separated by the T2A peptide, and expressed under the control of the Cbh promoter. After electroporation, native fluorescence of GFP from px458 was only partially visible at P6, moderately visible at P14 and bright at P21. To assess phenotypes at early ages, we co-electroporated px458 with pJS1, in which the mCherry coding sequence was expressed under the Ubiquitin promoter and visible as early as P2.

In px330, Cbh only drives Cas9 expression. For *in vivo* fluorescent co-labeling, we used either pJS1, in which mCherry was expressed under the Ubiquitin promoter, or pCAG-IRES-GFP, in which eGFP was expressed under the CAG promoter.

To knockdown NRL via RNAi, we inserted annealed oligonucleotides after the U6 promoter in pLL3.7 (Rubinson et al., 2003) digested with *HpaI* and *XhoI*. Oligonucleotides included an Nrl shRNA-encoding sequence designed by Cepko and colleagues (Matsuda and Cepko, 2004), labeled shRNA1, and a second sequence designed ourselves. Oligonucleotide sequences used, shRNA1: 5′-tGGTCCTGTCTCTATGGAAGttcaagagaCTTCCATAGAGACAGGACCttttttc – 3′; and 5′-tcgagaaaaaaGGTCCTGTCTCTATGGAAGtctcttgaaCTTCCATAGAGACAGGACCa – 3′; shRNA2: 5′-tGGGCCTCTTGGCTACTATTttcaagagaAATAGTAGCCAAGAGGCCCttttttc

– 3′; and 5′-
tcgagaaaaaGGGCCTCTTGGCTACTATTtctcttgaaAATAGTAGCCAAGAGGCCCa – 3′.

A dominant negative NRL coding sequence was designed based on truncated *Nrl* cDNA sequences analyzed by Swaroop and colleagues (Rehemtulla et al., 1996). The Nrl acidic region (amino acid residues 23–127) was excluded from cDNA amplification, while other domains (DNA binding domain) were kept. The following primers were used to amplify truncated NRL from the full cDNA: fwd: 5′-
TTGAGTCTAACCCAGGGCCAGATATGGCTTTCCCTCCCAGTCCCTTGGCTATGGAA
TATGTTAATGACTTTGATTTGATGAAGTTCGAA – 3′; rev: 5′ fwd: 5′-
TCTAGAGTCGCGGCCGCGATTCAGAGGAAGAGGTGTGTGTGGTCG – 3′. Truncated Nrl was subcloned after the T2A sequence in a plasmid bearing the CMV promoter and mKate2 followed by T2A. PCMV:mKate2 T2A was cut with NotI. The oligonucleotides above hold 25bp overhangs that allow recombination between the vector and oligonucleotides.

To spatially manipulate Cas9 expression, we used four promoters in px458. In the outer retina, we found that Cbh and Ubiquitin (Matsuda and Cepko, 2004) regulatory elements drive expression of fluorescent reporters in Rods, Bipolar Cells and Muller Glia. We used a 2.3 kb fragment of the Rhodopsin promoter to drive Cas9 expression in rods (Matsuda and Cepko, 2004; 2007), and a 1082 bp fragment containing a tandem repeat of an mGluR6-SV40 promoter (4XGrm6-Sv40) from the pAAV-4xGRM6-CatCh-EGFP vector (gift from Botand Roska) to drive Cas9 expression in ON BCs (van Wyk et al., 2017). Promoters were cloned between the KpnI and AgeI restriction sites in px458. In all cases, native fluorescence from GFP was visible by P21.

To multiplex sgRNAs, we modified the multiplex CRISPR vector system developed by Yamamoto and colleagues (Sakuma et al., 2014). We subcloned a BsaI site-bearing multiplex cassette (from the “A2” vector provided in the multiplex vector kit) into the XbaI site in px458, 190 bp downstream of the U6 promoter, creating a destination site for a new $U6^{prom}$:sgRNA cassette. We sequentially cloned sgRNAs into px330S and our new px458, then performed the multiplex reaction as published. All clones were confirmed by sequencing. Thus our single multiplexed vector expressed two guide RNAs, Cas9 and GFP.

CRISPR design: We designed at least two 20bp guide RNAs (sgRNAs) per gene, targeting either exon one or a common exon among splice isoforms using an algorithm developed by Zhang and colleagues (Hsu et al., 2013). Only guides with high specificity scores (>70), and low numbers of off-target sites were selected. SgRNAs were designed as complementary single strand oligonucleotides bearing CAAAG (forward oligo) or AAAC…C (reverse oligo) overhangs. Each complementary pair was annealed with T4 polynucleotide kinase and T4 ligase buffer, and ligated into BbsI restriction digest sites 3′ of the RNA polymerase III U6 promoter in the px458 plasmid (Ran et al., 2013). For complete list of oligonucleotide sequences used to design CRISPR/Cas9 vectors, see Table S6.

Electroporation—We electroporated retinas of neonatal pups (12–36 hours) *in vivo* using a protocol developed by Cepko and colleagues (Matsuda and Cepko, 2004; Wang et al.,

2014). Briefly, sharp end glass micropipettes are backfilled with 8–10uL of DNA mixed with Fast Green Dye (0.2X) using microloading pipette tips. DNA is diluted to a final concentration of 1ug/uL with 0.2X Tris-EDTA. We injected DNA into the subretinal space using a Femtojet express microinjector at 330 hPa for 1–2 pulses at 3.5 seconds. Five current pulses (80V, 50ms ON, 950ms OFF) were applied across the head using paddle electrodes.

Histology/Immunohistochemistry/Immunocytochemistry

Retinal tissue: Following enucleation, eyes were fixed in 4% paraformaldehyde for 45 minutes on ice. (For labeling with antibodies, mGluR6, Cacna1s, we found that fixation in 4% paraformaldehyde for 10 minutes at room temperature gave stronger signal.) Cryosections (20μm) were washed for 20 minutes with 1 X PBS, then permeabilized and blocked for 30 minutes in blocking solution containing 0.3% Triton X-100 and 3% Donkey Serum (or Goat Serum) in 1XPBS. Slides were then incubated with primary antibodies diluted in blocking solution overnight at 4°C in a humidified chamber. Primary antibodies were used at the following concentrations: anti-calbindin (1:2000), anti-S-opsin (1:500), anti-PSD-95 (1:400), anti-PKC (1:1000), anti-Secretagogin (1:2000), anti-Bassoon (1:600), anti-mGluR6 (1:1000), anti-GFP (1:2000), anti-Chx10 (1:500), anti-recoverin (1:4000), anti-RBPMS (1:50), CACNA1S (1:2000), Cone Arrestin (1:1000). After 3 washes of 5 minutes with 1XPBS, slides were incubated with Alexa Fluor secondary antibodies and when necessary treated with a nuclear counter-stain either TOPRO3 for 2 hours at room temperature or DAPI for 30 minutes at room temperature. Finally, slides were washed 3 times for 5 minutes each with 1XPBS and mounted in Fluoromount-G or VectaShield.

Retinal cultures on coverslips: Retinal cells on coverslips (see below) were fixed in 4% paraformaldehyde for 15 minutes, washed with 1XPBS and incubated in blocking buffer (see above) for 30 minutes at room temperature. Coverslips were incubated with primary antibodies overnight at 4C at the following concentrations: anti-rhodopsin 1:150 (EMD Millipore), anti-S-opsin 1:300 (Santa Cruz Biotechnology), anti-MAP2 1:1000 (Novocastra Laboratories), anti-TUJ1 1:500 (Neuromics), anti-Chx10 1:200 (Santa Cruz Biotechnology), anti-RBPMS 1:1000 (EMD Millipore), anti-Thy1 1:2000 (Abcam), anti glutamine synthetase 1:250 (Abcam), anti-AP2 1:100 (Abcam), anti-mCherry 1:1000 (Thermo Fisher), anti-Nr2e3 1:100 (a gift from Jeremy Nathans at Johns Hopkins), anti-recoverin 1:300 (EMD Millipore), anti-Ryk 1:150 (Abgent), and anti-Ryk 1:150 (a gift from Yimin Zou at UCSD). Stained coverslips were mounted in DAPI Fluoromount-G (SouthernBiotech).

Generation of mGluR6 antibody: The mGluR6 antibody was custom made through the Standard 70-day protocol from Thermo Fisher. Brielfy, two New Zealand White rabbits (Specific Pathogenic Free) were immunized with a peptide corresponding to the last 19 amino acids of rat mGluR6 as described in Morgans et al., 2006. The peptide sequence was conjugated with the immunogenic carrier keyhole limpet hemocyanin (KLH) and injected at 0.50mg. Booster injections were given every 14 days, and serum collection was performed on Day 56 from initial immunization. Immunoreactivity was determined by ELISA and the animal with the highest titer (200000ng/mL) was used in all experiments.

Photoreceptor cultures

Coverslip preparation: Flame-sterilized 12-mm round glass coverslips (Chemglass) were placed in sterile 24-well culture plates (Corning). Coverslips were then coated with a thin layer of Basement Membrane Extract using several steps. We first incubated the coverslips overnight in 1:4 poly-D-ornithine in ddH2O at 4C then rinsed once in ddH2O and air-dried for 5 minutes. Coverslips were then coated with 3 mg/mL Type 2 PathClear Cultrex BME (Trevigen) diluted in Dulbecco's Modified Eagle's Medium (DMEM; BioWhittaker Lonza). 100uL of BME suspension was applied to each coverslip using pre-chilled pipette tips and 5 mL tubes to avoid polymerization of BME. Coverslips were incubated at 37°C overnight. To generate thin gel-based layers, wells were incubated with ddH2O for 15 minutes at room temperature, then washed with 400uL DPBS immediately before seeding of retinal neurons. Coverslips were stored at 37°C with 400uL of culture medium (see below) until seeding.

Retinal dissociation: Retinas were dissected from P3 mice in Hank's Balanced Salt Solution (HBSS) (Ward's Science) on ice. Retinas were washed in Ca- Mg- free HBSS (Gibco) and incubated in papain solution (40 units papain suspension (Worthington), 300 units DNase I (Sigma), 10 mM HEPES in HBSS; 2.5 mL for 4 retinas) for 18 minutes at 37°C. Papain solution was removed and inactivated with 1 mL low-ovomucoid (LO) solution (1.5% BSA (Sigma) and 1.5% ovomucoid (Worthington)) in Eagle's minimal essential medium (MEM). Retinas were gently washed again with 1 mL LO, then 2X with 1% BSA in MEM (MEM-B). MEM-B was replaced with photoreceptor medium (PRM, see below) and retinal tissue was triturated 6X with a P1000 pipette tip. Cultures were seeded at 80,000 cell/well in 400uL PRM for low density experiments, and 400,000 cells/well for high-density experiments.

Magnetic cell sorting: To purify photoreceptors from dissociated retinal cells we used magnetic cell sorting. 4–6 retinas were dissociated as above with one exception, AMES buffer replaced MEM in all solutions. Retinal cells were suspended in 300μL 1% BSA/AMES and incubated with 2 μL rat anti-CD73 (Koso et al., 2009) or rat anti-CD133 (Lakowski et al., 2011) per 10^7 cells for 15 minutes at room temperature. Cells were washed with 1% BSA/AMES, centrifuged then resuspended in fresh 1% BSA/AMES, then incubated in 20 uL goat anti-rat magnetic microbeads per 10^7 cells for 15 minutes at room temperature. CD73/133-positive cells were separated from unbound cells in a magnetic column, then eluted by deactivating the magnet. Cells were seeded at 80,000 cells/well. Photoreceptor enrichment was confirmed by increased proportions of cells labeled by rod-specific antibodies (NR2E3, Rhodopsin) and a cone-specific antibody (S-opsin) and a decrease in proportions of cell labeled by non-photoreceptor markers (Bipolars cells: Chx10; Ganglion cells: RBPMS, Thy1; Muller Glia: Glutamine Synthetase, Amacrine cells: AP-2) (data not shown).

Culture conditions: Retinal neurons were cultured in in PRM, containing 2% B27, 50ng/mL brain-derived neurotrophic factor and 1X penicillin-streptomycin (Sigma) in Neurobasal (Gibco). Cultures were grown at 37°C in 5% CO2. After 24 hou rs, 100μL of media was removed, and cultures were replenished with 300μL of fresh PRM.

To analyze rod responses to Wnt proteins, cultures were first incubated at 37°C for 24 hours to allow adherence. Recombinant WNT5A, WNT5B or WNT3A were diluted in 0.2% BSA/PBS and added dropwise. A range of concentrations were tested for WNT5A/5B (100ng/mL, 500ng/mL, 1000ng/mL) and WNT3A (100ng/mL, 200ng/mL, 500ng/mL); however, we did not observe significant differences in outgrowth. Therefore, we used 100ng/mL of WNT protein for all experiments unless otherwise noted. Control cultures received 0.2% BSA/PBS alone.

Image Analysis

Retinal cryosections: Images of retinal cryosections were acquired by either an Olympus FluoView FV1000 or a Zeiss LSM780 confocal microscope. Single confocal planes are shown for all figures unless noted as maximum projections. FIJI 'Z-project' tool was used to generate maximum projections. Adobe Photoshop was used to adjust the levels of brightness and contrast.

Retinal cultures: Cultured retinal cells were imaged by the Zeiss Axio Imager Z1 (ApoTome) widefield microscope. Images of Ryk^{CRISPR} cultured cells (Figure 7E, S7) were acquired by an Olympus FluoView FV1000. Micrographs were analyzed in FIJI (https://fiji.sc/).

QUANTIFICATION AND STATISTICAL ANALYSIS

Phenotyping—In our pilot screen, 8/30 of total observed CRISPR knockouts exhibited abnormal outer retinas (Table S6). At least two images were scored (and averaged when quantified) for each CRISPR-mutant retina. All 8 phenotypes were observed in at least two animals cumulatively between both CRISPRs of each pair. We describe these phenotypes in Figures 5, 6 and S5. In all bar graphs, error bars represent standard error.

Neurite Outgrowth—Neurites in photoreceptor cultures were identified by the co-labeling of Rhodopsin, MAP2/TUJ1, and when necessary, RYK and/or mCherry. Rhodopsin labeling itself was sufficient to measure neurite length. Neurites were delineated and measured in FIJI by tracing neurites from the initial neurite protrusion until the terminal. In photoreceptor enriched cultures, only those neurites that did not contact other cells were included for quantification. Unless otherwise noted, a Student's T-test was performed to determine significance.

Bipolar CRISPR quantification—Retinas were co-transfected with pCAG-IRES-GFP and either Prkca CRISPR or Scgn CRISPR. The "spot" feature in Imaris (http://bitplane.com) was used to count the number of GFP-positive cells within the region of interest, the inner nuclear layer. Spots needed to have a diameter of 7μm and an ellipsoid shape of 5.93μm to be considered a bipolar cell. Next, the "surface" feature was used in the GFP channel to create a mask of the Scgn or PKC staining within the GFP transfected cells. The spot feature was used again with the same criteria as described above to count the number of cells in the masked Scgn-positive channel. Spots that co-localized in the GFP channel and the masked Scgn channel were counted as transfected cells that retained Scgn expression. The spot feature could not be used to count the number of PKC transfected cells

as this staining does not label the entire cell, and the program fails to recognize it as a "spot". The ratio of +GFP cells to either +PKC or +Scgn were plotted for the Control (no sgRNA) and Prkca CRISPR or Scgn CRISPR.

HC sprouting—An HC sprout was considered aberrant if it extended at least 5 μm apically (into the ONL) beyond the HC plexus. Sprouts were tallied per 20 μm (depth) × 200 μm (width) imaged stack.

Rod-cone distance—Distances were measured between each electroporated rod terminal and its closest cone terminal within a single optical plane (1 μm), then normalized to the average OPL width across the width of each image (~200 μm). Normalized distances were averaged among all animals mutagenized with either empty vector or each CRISPR.

Rod soma migation—Thicknesses of rod layers were measured in retinal cross sections. Rods were identified by their unique chromatin pattern as well as absence of labeling by the bipolar-marker, Chx10. Rods within the region bounded by the retinal pigment epithelium and OPL were denoted as ONL rods. Rods between the OPL and Chx10-expressing bipolar cells were denoted as INL rods. Thickness was measured by obtaining average Y-values across 300 μm-wide sections for the RPE, OPL and inner boundary of the INL rods.

DATA AND SOFTWARE AVAILABILITY

Raw and processed data files from RNA sequencing are available at NCBI GEO under the accession number GSE98838.

Supplementary Material

Refer to Web version on PubMed Central for supplementary material.

Acknowledgments

We thank X. William Yang for assistance; Xian-Jie Yang, Nick Brecha, Yimin Zou, and Anthony Wynshaw-Boris for reagents and mouse lines; Donghui Chen and Owen Witte for support; and Dorian Gunning for help with antibody production. We are particularly grateful for advice at early stages of our work from Felice Dunn and Rachel Wong. We thank the Sanes and Zipursky labs for comments on the manuscript.

This work was supported by the National Institute of Neurological Disorders and Stroke (T32NS048004) and the National Eye Institute (1K99EY028200) to E.Z., Helen Hay Whitney Foundation (E.Z.), Damon Runyon Fellowship (S.S.), and NIH R21 EY025421 (J.R.S.). Gerald Oppenheimer Family Foundation Center for Prevention of Eye Disease Award and Broad Stem Cell Research Center Innovation Award to M.M and S.L.Z. S.L.Z. is an Investigator of the Howard Hughes Medical Institute.

References

Andre P, Wang Q, Wang N, Gao B, Schilit A, Halford MM, Stacker SA, Zhang X, Yang Y. The Wnt coreceptor Ryk regulates Wnt/planar cell polarity by modulating the degradation of the core planar cell polarity component Vangl2. J Biol Chem. 2012; 287:44518–44525. [PubMed: 23144463]

Ashburner M, Ball CA, Blake JA, Botstein D, Butler H, Cherry JM, Davis AP, Dolinski K, Dwight SS, Eppig JT, et al. Gene ontology: tool for the unification of biology. The Gene Ontology Consortium Nat Genet. 2000; 25:25–29. [PubMed: 10802651]

Bai G, Chivatakarn O, Bonanomi D, Lettieri K, Franco L, Xia C, Stein E, Ma L, Lewcock JW, Pfaff SL. Presenilin-dependent receptor processing is required for axon guidance. Cell. 2011; 144:106–118. [PubMed: 21215373]

Behrens C, Schubert T, Haverkamp S, Euler T, Berens P. Connectivity map of bipolar cells and photoreceptors in the mouse retina. Elife. 2016; 5:1206.

Blanks JC, Adinolfi AM, Lolley RN. Synaptogenesis in the photoreceptor terminal of the mouse retina. The Journal of Comparative Neurology. 1974; 156:81–93. [PubMed: 4836656]

Brzezinski JA, Uoon Park K, Reh TA. Blimp1 (Prdm1) prevents re-specification of photoreceptors into retinal bipolar cells by restricting competence. Dev Biol. 2013; 384:194–204. [PubMed: 24125957]

Cao Y, Sarria I, Fehlhaber KE, Kamasawa N, Orlandi C, James KN, Hazen JL, Gardner MR, Farzan M, Lee A, et al. Mechanism for Selective Synaptic Wiring of Rod Photoreceptors into the Retinal Circuitry and Its Role in Vision. Neuron. 2015; 87:1248–1260. [PubMed: 26402607]

Carter-Dawson LD, LaVail MM. Rods and cones in the mouse retina. II Autoradiographic analysis of cell generation using tritiated thymidine. The Journal of Comparative Neurology. 1979; 188:263–272. [PubMed: 500859]

Chang B, Heckenlively JR, Bayley PR, Brecha NC, Davisson MT, Hawes NL, Hirano AA, Hurd RE, Ikeda A, Johnson BA, et al. The nob2 mouse, a null mutation in Cacna1f: anatomical and functional abnormalities in the outer retina and their consequences on ganglion cell visual responses. Vis Neurosci. 2006; 23:11–24. [PubMed: 16597347]

Chen Y, Lun ATL, Smyth GK. From reads to genes to pathways: differential expression analysis of RNA-Seq experiments using Rsubread and the edgeR quasi-likelihood pipeline. F1000Res. 2016; 5:1438. [PubMed: 27508061]

Christopherson KS, Ullian EM, Stokes CCA, Mullowney CE, Hell JW, Agah A, Lawler J, Mosher DF, Bornstein P, Barres BA. Thrombospondins are astrocyte-secreted proteins that promote CNS synaptogenesis. Cell. 2005; 120:421–433. [PubMed: 15707899]

Cong L, Ran FA, Cox D, Lin S, Barretto R, Habib N, Hsu PD, Wu X, Jiang W, Marraffini LA, et al. Multiplex genome engineering using CRISPR/Cas systems. Science. 2013; 339:819–823. [PubMed: 23287718]

de Wit J, Ghosh A. Specification of synaptic connectivity by cell surface interactions. Nat Rev Neurosci. 2016; 17:22–35. [PubMed: 26656254]

Dick O, tom Dieck S, Altrock WD, Ammermüller J, Weiler R, Garner CC, Gundelfinger ED, Brandstätter JH. The presynaptic active zone protein bassoon is essential for photoreceptor ribbon synapse formation in the retina. Neuron. 2003; 37:775–786. [PubMed: 12628168]

Dickins EM, Salinas PC. Wnts in action: from synapse formation to synaptic maintenance. Front Cell Neurosci. 2013; 7:162. [PubMed: 24223536]

Dobin A, Davis CA, Schlesinger F, Drenkow J, Zaleski C, Jha S, Batut P, Chaisson M, Gingeras TR. STAR: ultrafast universal RNA-seq aligner. Bioinformatics. 2013; 29:15–21. [PubMed: 23104886]

Dong X, You Y, Wu JQ. Building an RNA Sequencing Transcriptome of the Central Nervous System. Neuroscientist. 2016; 22:579–592. [PubMed: 26463470]

Drescher U, Kremoser C, Handwerker C, Löschinger J, Noda M, Bonhoeffer F. In vitro guidance of retinal ganglion cell axons by RAGS, a 25 kDa tectal protein related to ligands for Eph receptor tyrosine kinases. Cell. 1995; 82:359–370. [PubMed: 7634326]

Duan X, Krishnaswamy A, De la Huerta I, Sanes JR. Type II cadherins guide assembly of a direction-selective retinal circuit. Cell. 2014; 158:793–807. [PubMed: 25126785]

Dunn FA, Wong ROL. Diverse strategies engaged in establishing stereotypic wiring patterns among neurons sharing a common input at the visual system's first synapse. J Neurosci. 2012; 32:10306–10317. [PubMed: 22836264]

Dwyer ND, Manning DK, Moran JL, Mudbhary R, Fleming MS, Favero CB, Vock VM, O'Leary DDM, Walsh CA, Beier DR. A forward genetic screen with a thalamocortical axon reporter mouse yields novel neurodevelopment mutants and a distinct emx2 mutant phenotype. Neural Dev. 2011; 6:3. [PubMed: 21214893]

Fradkin LG, Dura JM, Noordermeer JN. Ryks: new partners for Wnts in the developing and regenerating nervous system. Trends Neurosci. 2010; 33:84–92. [PubMed: 20004982]

Fu X, Yang Y, Xu C, Niu Y, Chen T, Zhou Q, Liu JJ. Retrolinkin cooperates with endophilin A1 to mediate BDNF-TrkB early endocytic trafficking and signaling from early endosomes. Mol Biol Cell. 2011; 22:3684–3698. [PubMed: 21849472]

Fujimura N. WNT/β-Catenin Signaling in Vertebrate Eye Development. Front Cell Dev Biol. 2016; 4:138. [PubMed: 27965955]

Greene MJ, Kim JS, Seung HS, Wirers Eye. Analogous Convergence of Sustained and Transient Inputs in Parallel On and Off Pathways for Retinal Motion Computation. Cell Rep. 2016; 14:1892–1900. [PubMed: 26904938]

Halford MM, Armes J, Buchert M, Meskenaite V, Grail D, Hibbs ML, Wilks AF, Farlie PG, Newgreen DF, Hovens CM, et al. Ryk-deficient mice exhibit craniofacial defects associated with perturbed Eph receptor crosstalk. Nat Genet. 2000; 25:414–418. [PubMed: 10932185]

Hall AC, Lucas FR, Salinas PC. Axonal remodeling and synaptic differentiation in the cerebellum is regulated by WNT-7a signaling. Cell. 2000; 100:525–535. [PubMed: 10721990]

Haverkamp S, Wässle H. Immunocytochemical analysis of the mouse retina. The Journal of Comparative Neurology. 2000; 424:1–23. [PubMed: 10888735]

He X, Saint-Jeannet JP, Wang Y, Nathans J, Dawid I, Varmus H. A member of the Frizzled protein family mediating axis induction by Wnt-5A. Science. 1997; 275:1652–1654. [PubMed: 9054360]

Heidenreich M, Zhang F. Applications of CRISPR-Cas systems in neuroscience. Nat Rev Neurosci. 2016; 17:36–44. [PubMed: 26656253]

Hinds JW, Hinds PL. Differentiation of photoreceptors and horizontal cells in the embryonic mouse retina: an electron microscopic, serial section analysis. The Journal of Comparative Neurology. 1979; 187:495–511. [PubMed: 489789]

Holkers M, Maggio I, Henriques SFD, Janssen JM, Cathomen T, Gonçalves MAFV. Adenoviral vector DNA for accurate genome editing with engineered nucleases. Nat Methods. 2014; 11:1051–1057. [PubMed: 25152084]

Hollis ER, Ishiko N, Yu T, Lu CC, Haimovich A, Tolentino K, Richman A, Tury A, Wang SH, Pessian M, et al. Ryk controls remapping of motor cortex during functional recovery after spinal cord injury. Nat Neurosci. 2016; 19:697–705. [PubMed: 27065364]

Hoon M, Okawa H, Santina, Della L, Wong ROL. Functional architecture of the retina: development and disease. Prog Retin Eye Res. 2014; 42:44–84. [PubMed: 24984227]

Hsu PD, Scott DA, Weinstein JA, Ran FA, Konermann S, Agarwala V, Li Y, Fine EJ, Wu X, Shalem O, et al. DNA targeting specificity of RNA-guided Cas9 nucleases. Nature Biotechnology. 2013; 31:827–832.

Huckfeldt RM, Schubert T, Morgan JL, Godinho L, Di Cristo G, Huang ZJ, Wong ROL. Transient neurites of retinal horizontal cells exhibit columnar tiling via homotypic interactions. Nat Neurosci. 2009; 12:35–43. [PubMed: 19060895]

Jeon CJ, Strettoi E, Masland RH. The major cell populations of the mouse retina. Journal of Neuroscience. 1998; 18:8936–8946. [PubMed: 9786999]

Kalashnikova E, Lorca RA, Kaur I, Barisone GA, Li B, Ishimaru T, Trimmer JS, Mohapatra DP, Díaz E. SynDIG1: an activity-regulated, AMPA- receptor-interacting transmembrane protein that regulates excitatory synapse development. Neuron. 2010; 65:80–93. [PubMed: 20152115]

Katoh K, Omori Y, Onishi A, Sato S, Kondo M, Furukawa T. Blimp1 suppresses Chx10 expression in differentiating retinal photoreceptor precursors to ensure proper photoreceptor development. J Neurosci. 2010; 30:6515–6526. [PubMed: 20463215]

Kay JN, Chu MW, Sanes JR. MEGF10 and MEGF11 mediate homotypic interactions required for mosaic spacing of retinal neurons. Nature. 2012; 483:465–469. [PubMed: 22407321]

Keeble TR, Halford MM, Seaman C, Kee N, Macheda M, Anderson RB, Stacker SA, Cooper HM. The Wnt receptor Ryk is required for Wnt5a-mediated axon guidance on the contralateral side of the corpus callosum. J Neurosci. 2006; 26:5840–5848. [PubMed: 16723543]

Kim GH, Her JH, Han JK. Ryk cooperates with Frizzled 7 to promote Wnt11-mediated endocytosis and is essential for Xenopus laevis convergent extension movements. J Cell Biol. 2008; 182:1073–1082. [PubMed: 18809723]

Kim JW, Yang HJ, Brooks MJ, Zelinger L, Karakülah G, Gotoh N, Boleda A, Gieser L, Giuste F, Whitaker DT, et al. NRL-Regulated Transcriptome Dynamics of Developing Rod Photoreceptors. Cell Rep. 2016; 17:2460–2473. [PubMed: 27880916]

Klassen MP, Shen K. Wnt signaling positions neuromuscular connectivity by inhibiting synapse formation in C. elegans. Cell. 2007; 130:704–716. [PubMed: 17719547]

Kolodkin AL, Tessier-Lavigne M. Mechanisms and molecules of neuronal wiring: a primer. Cold Spring Harbor Perspectives in Biology. 2011; 3:a001727–a001727. [PubMed: 21123392]

Koso H, Minami C, Tabata Y, Inoue M, Sasaki E, Satoh S, Watanabe S. CD73, a novel cell surface antigen that characterizes retinal photoreceptor precursor cells. Invest Ophthalmol Vis Sci. 2009; 50:5411–5418. [PubMed: 19515998]

Koulen P, Fletcher EL, Craven SE, Bredt DS, Wässle H. Immunocytochemical localization of the postsynaptic density protein PSD-95 in the mammalian retina. Journal of Neuroscience. 1998; 18:10136–10149. [PubMed: 9822767]

Lakowski J, Han YT, Pearson RA, Gonzalez-Cordero A, West EL, Gualdoni S, Barber AC, Hubank M, Ali RR, Sowden JC. Effective transplantation of photoreceptor precursor cells selected via cell surface antigen expression. Stem Cells. 2011; 29:1391–1404. [PubMed: 21774040]

Le YZ, Ash JD, Al-Ubaidi MR, Chen Y, Ma JX, Anderson RE. Targeted expression of Cre recombinase to cone photoreceptors in transgenic mice. Mol Vis. 2004; 10:1011–1018. [PubMed: 15635292]

Li S, Chen D, Sauvé Y, McCandless J, Chen YJ, Chen CK. Rhodopsin-iCre transgenic mouse line for Cre-mediated rod-specific gene targeting. Genesis. 2005; 41:73–80. [PubMed: 15682388]

Lijam N, Paylor R, McDonald MP, Crawley JN, Deng CX, Herrup K, Stevens KE, Maccaferri G, McBain CJ, Sussman DJ, et al. Social interaction and sensorimotor gating abnormalities in mice lacking Dvl1. Cell. 1997; 90:895–905. [PubMed: 9298901]

Lin S, Baye LM, Westfall TA, Slusarski DC. Wnt5b-Ryk pathway provides directional signals to regulate gastrulation movement. J Cell Biol. 2010; 190:263–278. [PubMed: 20660632]

Linhoff MW, Laurén J, Cassidy RM, Dobie FA, Takahashi H, Nygaard HB, Airaksinen MS, Strittmatter SM, Craig AM. An unbiased expression screen for synaptogenic proteins identifies the LRRTM protein family as synaptic organizers. Neuron. 2009; 61:734–749. [PubMed: 19285470]

Liu Y, Shi J, Lu CC, Wang ZB, Lyuksyutova AI, Song XJ, Song X, Zou Y. Ryk-mediated Wnt repulsion regulates posterior-directed growth of corticospinal tract. Nat Neurosci. 2005; 8:1151–1159. [PubMed: 16116452]

Lu W, Yamamoto V, Ortega B, Baltimore D. Mammalian Ryk is a Wnt coreceptor required for stimulation of neurite outgrowth. Cell. 2004; 119:97–108. [PubMed: 15454084]

Macosko EZ, Basu A, Satija R, Nemesh J, Shekhar K, Goldman M, Tirosh I, Bialas AR, Kamitaki N, Martersteck EM, et al. Highly Parallel Genome-wide Expression Profiling of Individual Cells Using Nanoliter Droplets. Cell. 2015; 161:1202–1214. [PubMed: 26000488]

Matsuda T, Cepko CL. Electroporation and RNA interference in the rodent retina in vivo and in vitro. Proc Natl Acad Sci USa. 2004; 101:16–22. [PubMed: 14603031]

Matsuda T, Cepko CL. Controlled expression of transgenes introduced by in vivo electroporation. Proc Natl Acad Sci USa. 2007; 104:1027–1032. [PubMed: 17209010]

Matsuoka RL, Jiang Z, Samuels IS, Nguyen-Ba-Charvet KT, Sun LO, Peachey NS, Chédotal A, Yau KW, Kolodkin AL. Guidance-cue control of horizontal cell morphology, lamination, and synapse formation in the mammalian outer retina. J Neurosci. 2012; 32:6859–6868. [PubMed: 22593055]

Maurel P, Rauch U, Flad M, Margolis RK, Margolis RU. Phosphacan, a chondroitin sulfate proteoglycan of brain that interacts with neurons and neural cell-adhesion molecules, is an extracellular variant of a receptor-type protein tyrosine phosphatase. Proc Natl Acad Sci USa. 1994; 91:2512–2516. [PubMed: 7511813]

Mears AJ, Kondo M, Swain PK, Takada Y, Bush RA, Saunders TL, Sieving PA, Swaroop A. Nrl is required for rod photoreceptor development. Nat Genet. 2001; 29:447–452. [PubMed: 11694879]

Morgan JL, Dhingra A, Vardi N, Wong ROL. Axons and dendrites originate from neuroepithelial-like processes of retinal bipolar cells. Nat Neurosci. 2006; 9:85–92. [PubMed: 16341211]

Morgans CW, Ren G, Akileswaran L. Localization of nyctalopin in the mammalian retina. Eur J Neurosci. 2006; 23:1163–1171. [PubMed: 16553780]

Nakamoto M, Cheng HJ, Friedman GC, McLaughlin T, Hansen MJ, Yoon CH, O'Leary DD, Flanagan JG. Topographically specific effects of ELF-1 on retinal axon guidance in vitro and retinal axon mapping in vivo. Cell. 1996; 86:755–766. [PubMed: 8797822]

Olney JW. An electron microscopic study of synapse formation, receptor outer segment development, and other aspects of developing mouse retina. Invest Ophthalmol. 1968; 7:250–268. [PubMed: 5655873]

Pang JJ, Gao F, Lem J, Bramblett DE, Paul DL, Wu SM. Direct rod input to cone BCs and direct cone input to rod BCs challenge the traditional view of mammalian BC circuitry. Proc Natl Acad Sci USa. 2010; 107:395–400. [PubMed: 20018684]

Puthussery T, Gayet-Primo J, Taylor WR. Localization of the calcium-binding protein secretagogin in cone bipolar cells of the mammalian retina. Journal of Comparative Neurology. 2010; 518:513–525. [PubMed: 20020539]

Ran FA, Hsu PD, Wright J, Agarwala V, Scott DA, Zhang F. Genome engineering using the CRISPR-Cas9 system. Nat Protoc. 2013; 8:2281–2308. [PubMed: 24157548]

Rehemtulla A, Warwar R, Kumar R, Ji X, Zack DJ, Swaroop A. The basic motif-leucine zipper transcription factor Nrl can positively regulate rhodopsin gene expression. Proc Natl Acad Sci USa. 1996; 93:191–195. [PubMed: 8552602]

Ribic A, Liu X, Crair MC, Biederer T. Structural organization and function of mouse photoreceptor ribbon synapses involve the immunoglobulin protein synaptic cell adhesion molecule 1. Journal of Comparative Neurology. 2014; 522:900–920. [PubMed: 23982969]

Rich KA, Zhan Y, Blanks JC. Migration and synaptogenesis of cone photoreceptors in the developing mouse retina. The Journal of Comparative Neurology. 1997; 388:47–63. [PubMed: 9364238]

Robinson MD, McCarthy DJ, Smyth GK. edgeR: a Bioconductor package for differential expression analysis of digital gene expression data. Bioinformatics. 2010; 26:139–140. [PubMed: 19910308]

Roesch K, Jadhav AP, Trimarchi JM, Stadler MB, Roska B, Sun BB, Cepko CL. The transcriptome of retinal Müller glial cells. Journal of Comparative Neurology. 2008; 509:225–238. [PubMed: 18465787]

Rowan S, Cepko CL. Genetic analysis of the homeodomain transcription factor Chx10 in the retina using a novel multifunctional BAC transgenic mouse reporter. Dev Biol. 2004; 271:388–402. [PubMed: 15223342]

Rubinson DA, Dillon CP, Kwiatkowski AV, Sievers C, Yang L, Kopinja J, Rooney DL, Zhang M, Ihrig MM, McManus MT, et al. A lentivirus-based system to functionally silence genes in primary mammalian cells, stem cells and transgenic mice by RNA interference. Nat Genet. 2003; 33:401–406. [PubMed: 12590264]

Sakuma T, Nishikawa A, Kume S, Chayama K, Yamamoto T. Multiplex genome engineering in human cells using all-in-one CRISPR/Cas9 vector system. Scientific Reports. 2014; 4

Samuel MA, Voinescu PE, Lilley BN, de Cabo R, Foretz M, Viollet B, Pawlyk B, Sandberg MA, Vavvas DG, Sanes JR. LKB1 and AMPK regulate synaptic remodeling in old age. Nat Neurosci. 2014; 17:1190–1197. [PubMed: 25086610]

Sanes JR, Zipursky SL. Design principles of insect and vertebrate visual systems. Neuron. 2010; 66:15–36. [PubMed: 20399726]

Serafini T, Kennedy TE, Galko MJ, Mirzayan C, Jessell TM, Tessier-Lavigne M. The netrins define a family of axon outgrowth-promoting proteins homologous to C. elegans UNC-6. Cell. 1994; 78:409–424. [PubMed: 8062384]

Shalem O, Sanjana NE, Hartenian E, Shi X, Scott DA, Mikkelsen TS, Heckl D, Ebert BL, Root DE, Doench JG, et al. Genome-scale CRISPR-Cas9 knockout screening in human cells. Science. 2014; 343:84–87. [PubMed: 24336571]

Shekhar K, Lapan SW, Whitney IE, Tran NM, Macosko EZ, Kowalczyk M, Adiconis X, Levin JZ, Nemesh J, Goldman M, et al. Comprehensive Classification of Retinal Bipolar Neurons by Single-Cell Transcriptomics. Cell. 2016; 166:1308–1323. e1330. [PubMed: 27565351]

Sherry DM, Wang MM, Bates J, Frishman LJ. Expression of vesicular glutamate transporter 1 in the mouse retina reveals temporal ordering in development of rod vs. cone and ON vs OFF circuits. The Journal of Comparative Neurology. 2003; 465:480–498. [PubMed: 12975811]

Shinmyo Y, Tanaka S, Tsunoda S, Hosomichi K, Tajima A, Kawasaki H. CRISPR/Cas9-mediated gene knockout in the mouse brain using in utero electroporation. Scientific Reports. 2016; 6:20611. [PubMed: 26857612]

Siegert S, Cabuy E, Scherf BG, Kohler H, Panda S, Le YZ, Fehling HJ, Gaidatzis D, Stadler MB, Roska B. Transcriptional code and disease map for adult retinal cell types. Nat Neurosci. 2012; 15:487–95. S1–2. [PubMed: 22267162]

Soto F, Watkins KL, Johnson RE, Schottler F, Kerschensteiner D. NGL-2 Regulates Pathway-Specific Neurite Growth and Lamination, Synapse Formation, and Signal Transmission in the Retina. Journal of Neuroscience. 2013; 33:11949–11959. [PubMed: 23864682]

Swiech L, Heidenreich M, Banerjee A, Habib N, Li Y, Trombetta J, Sur M, Zhang F. In vivo interrogation of gene function in the mammalian brain using CRISPR-Cas9. Nature Biotechnology. 2015; 33:102–106.

Uezu A, Kanak DJ, Bradshaw TWA, Soderblom EJ, Catavero CM, Burette AC, Weinberg RJ, Soderling SH. Identification of an elaborate complex mediating postsynaptic inhibition. Science. 2016; 353:1123–1129. [PubMed: 27609886]

Umemori H, Linhoff MW, Ornitz DM, Sanes JR. FGF22 and its close relatives are presynaptic organizing molecules in the mammalian brain. Cell. 2004; 118:257–270. [PubMed: 15260994]

van Wyk M, Hulliger EC, Girod L, Ebneter A, Kleinlogel S. Present Molecular Limitations of ON-Bipolar Cell Targeted Gene Therapy. Front Neurosci. 2017; 11:161. [PubMed: 28424574]

Veleri S, Nellissery J, Mishra B, Manjunath SH, Brooks MJ, Dong L, Nagashima K, Qian H, Gao C, Sergeev YV, et al. REEP6 mediates trafficking of a subset of Clathrin-coated vesicles and is critical for rod photoreceptor function and survival. Hum Mol Genet. 2017; 26:2218–2230. [PubMed: 28369466]

Wang S, Sengel C, Emerson MM, Cepko CL. A gene regulatory network controls the binary fate decision of rod and bipolar cells in the vertebrate retina. Dev Cell. 2014; 30:513–527. [PubMed: 25155555]

Witze ES, Litman ES, Argast GM, Moon RT, Ahn NG. Wnt5a control of cell polarity and directional movement by polarized redistribution of adhesion receptors. Science. 2008; 320:365–9. [PubMed: 18420933]

Yamagata M, Weiner JA, Sanes JR. Sidekicks: synaptic adhesion molecules that promote lamina-specific connectivity in the retina. Cell. 2002; 110:649–660. [PubMed: 12230981]

Young RW. Cell differentiation in the retina of the mouse. Anat Rec. 1985; 212:199–205. [PubMed: 3842042]

Yu H, Ye X, Guo N, Nathans J. Frizzled 2 and frizzled 7 function redundantly in convergent extension and closure of the ventricular septum and palate: evidence for a network of interacting genes. Development. 2012; 139:4383–4394. [PubMed: 23095888]

Yue Q, Wagstaff L, Yang X, Weijer C, Münsterberg A. Wnt3a-mediated chemorepulsion controls movement patterns of cardiac progenitors and requires RhoA function. Development. 2008; 135:1029–1037. [PubMed: 18256196]

Zhang C, Kolodkin AL, Wong RO, James RE. Establishing Wiring Specificity in Visual System Circuits: From the Retina to the Brain. Annu Rev Neurosci. 2017; 40 annurev–neuro–072116–031607.

Highlights

- Lamination in synaptic neuropil of the outer retina arises in a series of steps
- RNAseq reveals distinct cell surface genes expressed by 4 outer retinal cell types
- CRISPR-based electroporation inactivates genes in photoreceptor and bipolar neurons
- Wnt5 acts through Ryk to regulate neurophil formation in the outer retina

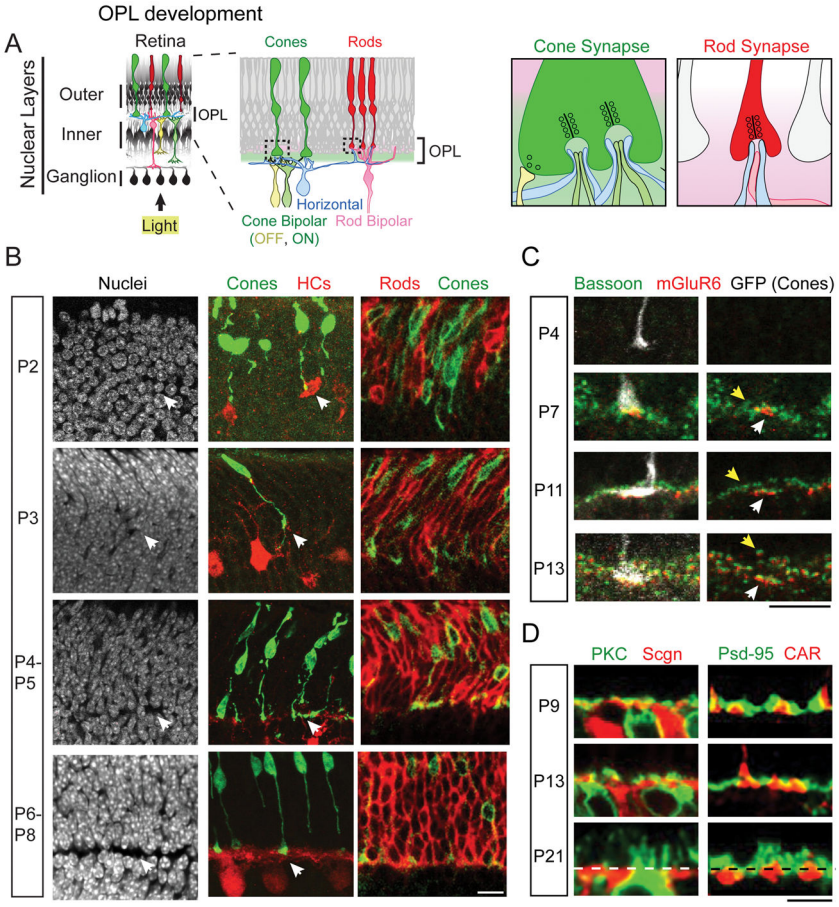

Figure 1. Development of the OPL

A. Schematic of the adult retina.

B. Generation of the OPL. Rods (anti-Rhodopsin) and cones (anti-S-opsin) are present at P2. At P4–5, gaps between the nuclear layers coincides with photoreceptor terminals (arrowhead). By P6–8, the OPL is continuous. Nuclei labeled with TOPRO3 and HCs with calbindin; left and center panels (max projections) show the same fields. Scale bar, 10 μm.

C. Synaptogenesis. Sparsely labeled cone terminals (Hb9:GFP transgene) are visible by P4. Juxtaposition of presynaptic Bassoon and postsynaptic mGluR6 first appears in cones (white arrowheads) at P7 and in rods (yellow arrowheads) by P13. Scale bar, 10 μm.

D. Segregation of rod and cone terminal layers. Dendrites of CBCs (Scgn) and RBCs (PKC) overlap as do rod (PSD-95) and cone (CAR) terminals at P9. Rod and cone synapses segregate into separate layers between P13 and P21. Although PSD-95 is expressed by both rods and cones, its uniquely focal localization in rod terminals allowed us to use it as a marker for rod terminal positioning. Scale bar, 10 μm.

See also Figure S1.

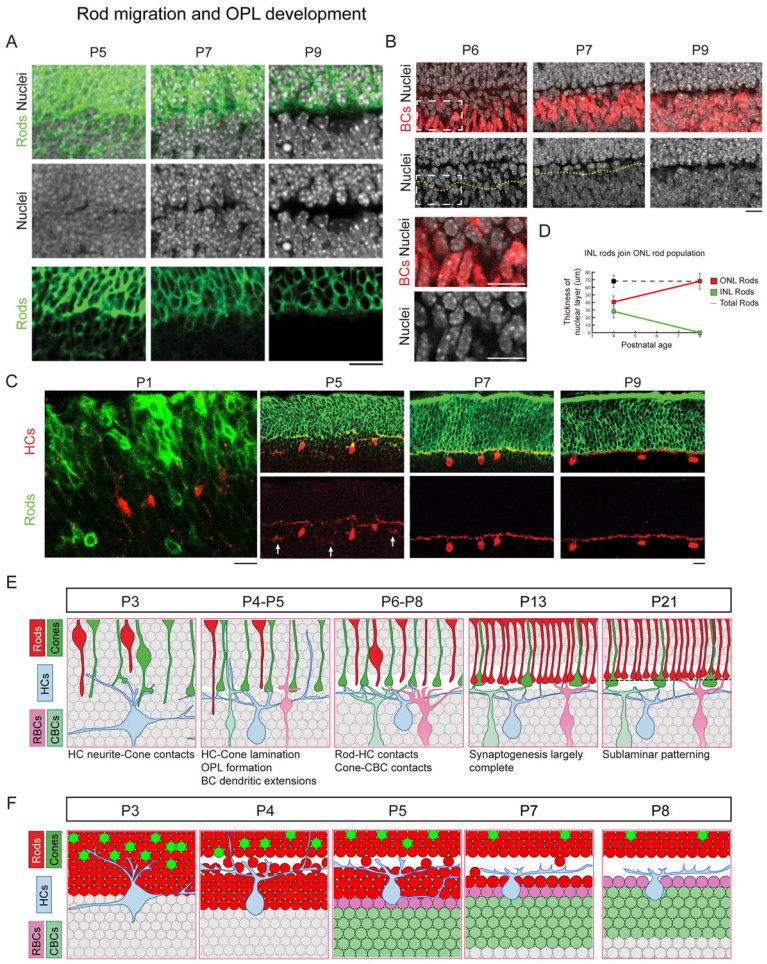

Figure 2. Cellular rearrangements during OPL development

A, B. Rod somata are transiently present in the developing INL. Rod somata (anti-Rhodopsin) are present below the developing OPL until P7. By P9, INL cells juxtaposing the OPL are BCs (anti-Chx10). Nuclei labeled with TOPRO3. Scale bar, 10 μm.

C. Secondary HC processes (anti-CALB) appear at P5 and join the OPL by P7. Rod somata are initially intermingled with those of HCs (P1), then also found between the HC processes (P5) as shown by arrows, and finally exclusive to the ONL (P7, P9). Scale bar, 10 μm.

D. The ONL gains an equal amount of rod somata as are lost from INL; consistent with rods migrating from the INL into the ONL. Error bars = Standard error. Thickness determined in cross-section, n=3 for each measurement.

E. Overview of OPL development, summarizing data from Figure 1B–D.

F. Overview of cellular rearrangements during OPL development, summarizing data from panels A–D.

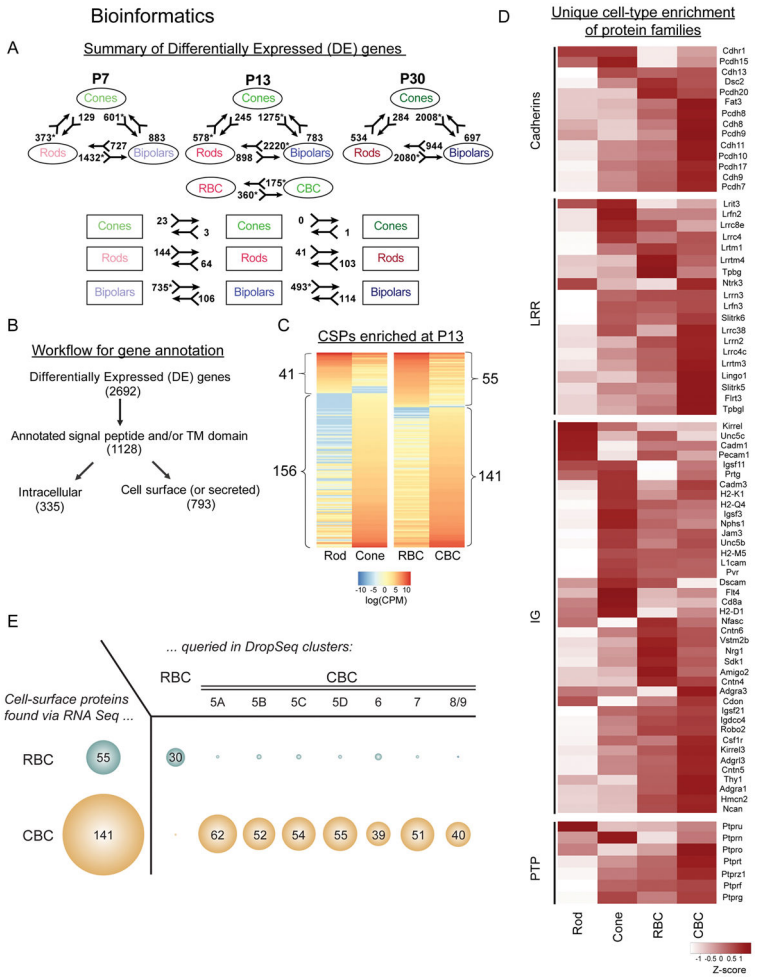

Figure 3. Analysis of RNA sequencing data

A. Summary of Differentially Expressed (DE) genes. Asterisk denotes significant overrepresentation of genes associated with GO term “plasma membrane”.

B. Annotation of cell surface and secreted proteins performed on merged DE gene list identified in all pairwise comparisons.

C. Cell surface and secreted proteins (CSPs) differentially enriched in rods and cones, and between RBCs and CBCs at P13.

D. Expression patterns of DE cell surface proteins of selected protein families at P13. LRR = Leucine Rich Repeat, PTP = Protein Receptor Tyrosine Phosphatases, and IG = immunoglobulin-superfamily proteins. Z-scores are plotted for each gene.

E. Comparison of RBC and CBC enriched CSPs with ON bipolar types (BC5-9) from DropSeq data.

See also Figures S2, S3

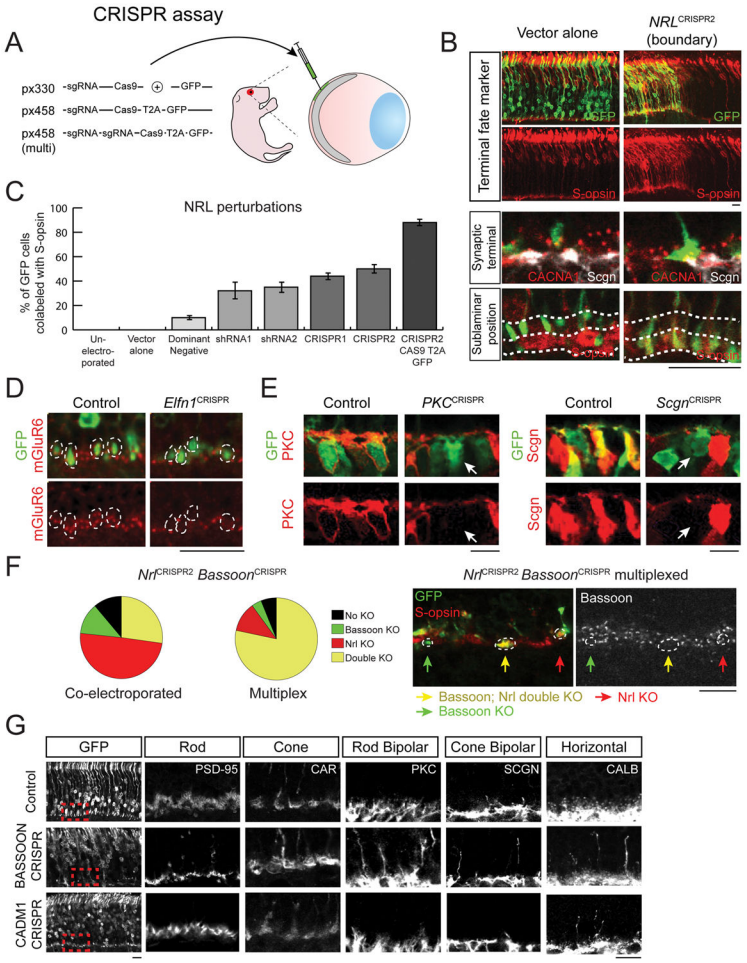

Figure 4. CRISPR/Cas9 Gene knockout in the postnatal retina

A. Schematic of CRISPR-Cas9 knock out vectors. DNA (green) is injected into the subretinal space of newborn CD1 pups and delivered into dividing cells via electroporation.

B. Conversion of rods to cone-like cells (cods) via Nrl-CRISPR. Transformed cells (green) express a cone specific opsin (S-opsin; red cells). By contrast, transfected control cells do not express S-opsin (i.e. no yellow cells). In addition, cod axon terminals terminate in the cone layer of the OPL, display enhanced clustering of a postsynaptic marker (anti-Cacna1), and form contacts to cone bipolars (anti-Scgn). Terminal fate marker images are max projections. Scale bar, 10μm.

C. S-opsin immunoreactivity of cells electroporated with constructs that attenuate Nrl function. Dominant negative transgene against Nrl; shRNA directed towards Nrl; CRISPR: gRNA directed toward Nrl on a separate plasmid from GFP; CRISPR2 Cas9 T2A GFP: all transgenes on the same plasmid. Error bars indicate standard error in this and all other figures.

D. Loss of mGluR6 protein (red) juxtaposing terminals of rods (dotted circles) transfected with an Elfn1 CRISPR (GFP; green). Scale bar, 10μm.

E. Knockout of Prkca (PKC) in RBCs and Secretagogin (Scgn) in CBCs (arrowheads). Cas9 was expressed from a mGluR6 promoter. See Figure S4C for quantification. Retinas were examined at P9. Scale bar, 10μm.

F. Efficiency of double CRISPR knockouts. Left: Co-electroporation of Nrl and Bassoon CRISPR. Right: Multi-plex construct. Charts represent average values scored for at least 3 animals under each condition. Red arrow, a cell in which only Nrl, but not Bassoon, was knocked out. Green arrow, a cell in which only Bassoon was knocked out; Yellow arrow, both Nrl and Bassoon were knocked out. Scale bar = 10 μm.

G. Mutations differentially affect sprouting of neurites. Bassoon CRISPR (middle) show retraction of rod terminals (PSD-95), sprouting of RBCs (PKC), CBCs (SCGN), and HCs (CALB) but no cone defects (CAR). Cadm1 CRISPR (bottom) show only HC sprouting (CALB). Control CRISPR show neither retraction nor sprouting (top). Panels showing cell-type marker expression are zoomed regions of red dotted boxes. Images are max projections. Scale bar, 10μm.

See also Figures S4

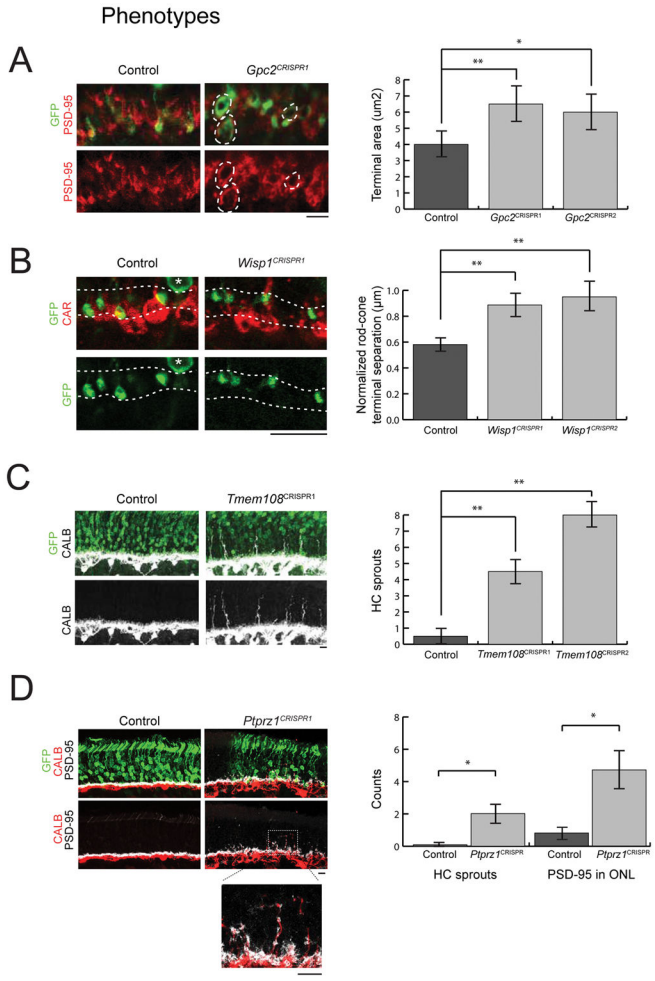

Figure 5. Several CRISPR/Cas9-based mosaic knockouts disrupt development of the outer retina

A. Enlarged rod terminals in *Gpc-2*$^{\text{CRISPR}}$ animals. Images show *Gpc-2*$^{\text{CRISPR}}$ transfected cells (green) and rod terminals (PSD-95, red). Scale bar, 10µm. Significance determined by single-tailed Student's t-test (** = p<0.01, * = p<.05).

B. Misplaced rod terminals in *Wisp-1*$^{\text{CRISPR}}$ animals. Images show *Wisp-1*$^{\text{CRISPR}}$ transfected rods (green) and cone terminals (CAR, red). White dotted lines demarcate the OPL region populated with rod terminals. A rod soma is labeled with a white star. Scale bar, 10µm. Significance determined by single-tailed Student's t-test (** = p<0.01).

C. HC sprouting in *Tmem108*$^{\text{CRISPR}}$ animals. Max projection images show *Tmem108*$^{\text{CRISPR}}$ cells (green) and HCs (CALB, white). Scale bar, 10µm. Significance determined by single-tailed Student's t-test (** = p<0.01).

D. Ectopic PSD-95 expression and HC sprouting in *Ptprz1*$^{\text{CRISPR}}$ animals. Max projections show *Ptprz1*$^{\text{CRISPR}}$ (green), HCs (CALB, red), and photoreceptor terminals (PSD-95, white). Scale bar, 10µm. Counts refer to number of PSD-95 puncta or HC sprouts. *Ptprz1*$^{\text{CRISPR}}$ represents average counts of two CRISPRs. Right panel: zoomed region of white dotted box. Significance determined by single-tailed Student's t-test (* = p<0.05).

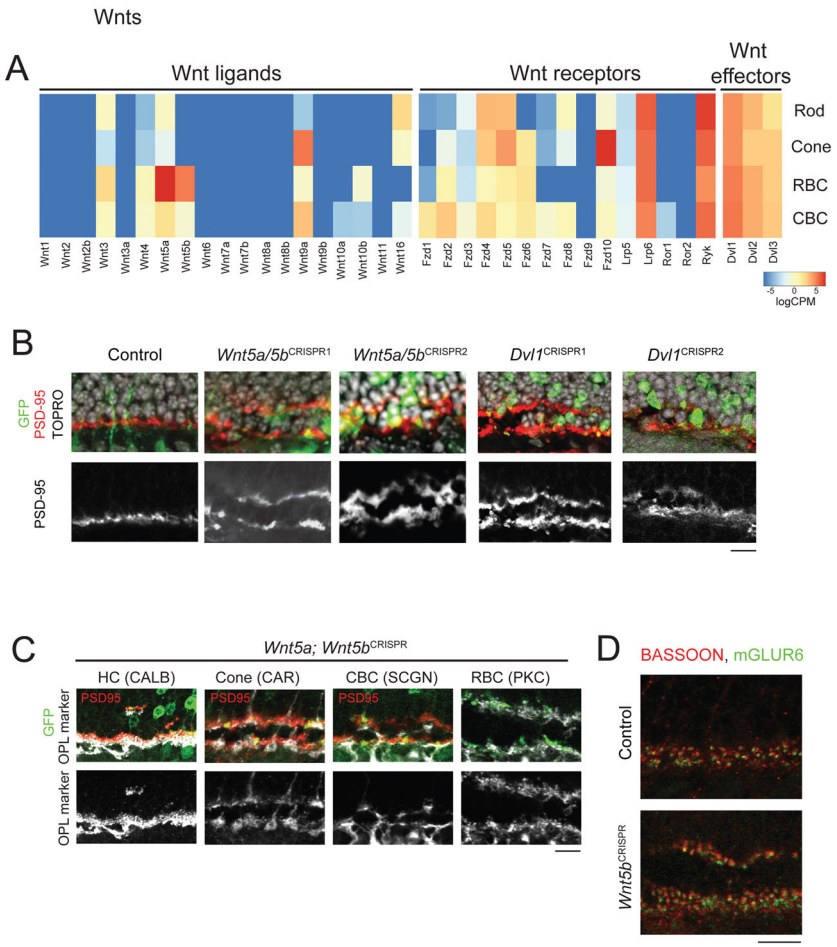

Figure 6. CRISPR-Cas9 mediated knockout of Wnt5 induces a second OPL

A. Expression patterns of Wnt pathway components in rods, cones, RBCs and CBCs at P13. Values are shown as mean logCPM.

B. CRISPR double knock out of Wnt5a/5b, and single knock outs of Dvl1 induce a second neuropil in the outer retina. Retinas were assayed at P21. GFP, electroporated cells; anti-PSD-95, photoreceptor terminals; TOPRO3, nuclei. Controls (left panels), were electroporated with an empty CRISPR vector. Scale bar, 10 μm.

C. Composition of the ectopic neuropil in Wnt5a/5b CRISPR-knockout retinas. In addition to rod terminals, the ectopic neuropil contains cone axon terminals and processes of horizontal cells (CALB), CBCs (SCGN), and RBCs (PKC). Retinas stained at P21. Scale bar, 10 μm.

D. Synapses are formed in the ectopic OPL: Retinas were stained with Bassoon (presynaptic) and mGluR6 (postsynaptic). Bassoon and mGluR6 puncta remain juxtaposed in the Wnt5a/b^{CRISPR} -induced ectopic OPL, indicating close apposition of pre- and postsynaptic structures. Scale bar, 10 μm.

See also Figure S5, S6

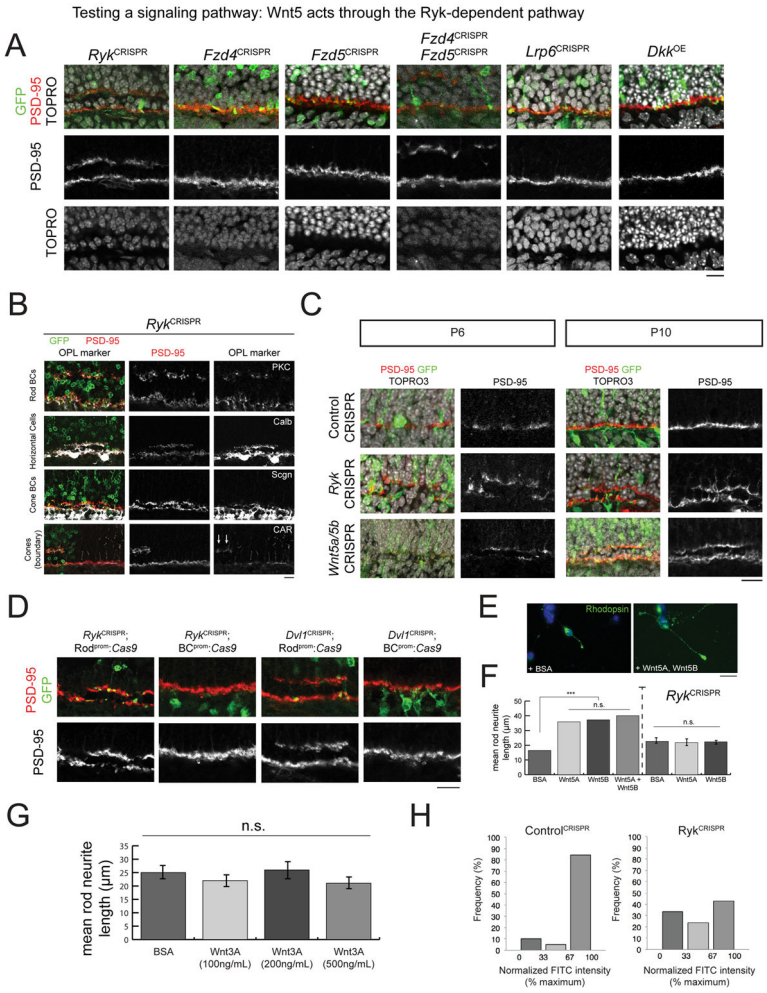

Figure 7. Wnt5 acts through the Ryk-dependent pathway

A. CRISPR knockouts of non-canonical Wnt receptor Ryk or of both Fzd4 and Fzd5 phenocopied Wnt5a/5b knockouts. In contrast, genetic disruption of the canonical Wnt pathway displayed no abnormalities. Three to six retinas analyzed per mutant. Markers used: PSD-95, photoreceptor terminals; GFP, electroporated patches; and TOPRO3, nuclear marker. Scale bar, 10 μm.

B. The ectopic OPL stained for processes of RBCs (PKC), HCs (CALB), CBCs (SCGN), and Cones (CAR) in addition to rod terminals (middle panels; PSD-95). White arrows indicate cone terminals within Ryk CRISPR-induced lamina. Scale bar, 10 μm.

C. Ectopic laminae were observed as early as P6 in both CRISPR-mediated knockouts of Ryk and double knockouts of Wnt5a/5b. Markers: OPL, PSD-95; transfected cells, GFP; and nuclei, TOPRO3. Scale bar, 10 μm.

D. A second neuropil was formed when Ryk was knocked out of rods by targeting Cas9 expression using the Rhodopsin promoter (Rod^{prom}), but not when targeting to bipolar cells (BC^{prom}). Markers: OPL, PSD-95; electroporated cells, GFP. Likewise, a duplicated OPL was observed when Dvl1 knockout was limited to rods but not to bipolar cells. Scale bar, 10 μm.

E. Three day retina cultures grown in bath-applied BSA, Wnt5A, Wnt5B or Wnt5A/5B. Wnt ligands were bath applied at a total concentration of 100 ng/mL (for Wnt5a/5b, 50 ng/mL each). Rods were distinguished by Rhodopsin staining. Nuclei stained with DAPI (blue). Scale bar, 10 μm.

F. Quantification of E (Left). From left to right: n (cells/cultures) = 64/4, 56/4, 70/2, 57/2. Neurite outgrowth in control and Ryk knockout cultured rods (Right). Wnt5a and Wnt5b were bath applied at a concentration of 100ng/mL. From left to right: n (cells/cultures) = 34/2, 41/2, 39/2. Significance determined by two-tailed Student's T-test comparison between test condition and control (BSA). *** = p<.001; n.s. = not significant.

G. Three-day retinal cultures grown with bath-applied BSA or Wnt3a. From left to right n (cells/cultures): 30/2, 31/2, 32/2, 35/2. Significance determined by two-tailed Student's T-test comparison between test condition and control (BSA). n.s. = not significant.

H. Ryk^{CRISPR} reduces RYK expression in cultured rods. Histograms show Ryk signal intensity for rhodopsin-positive cells that also express mCherry. Control sgRNA: n=3 cultures, 77 total cells; Ryk sgRNA: n=3 cultures, 84 total cells.

See also Figure S7

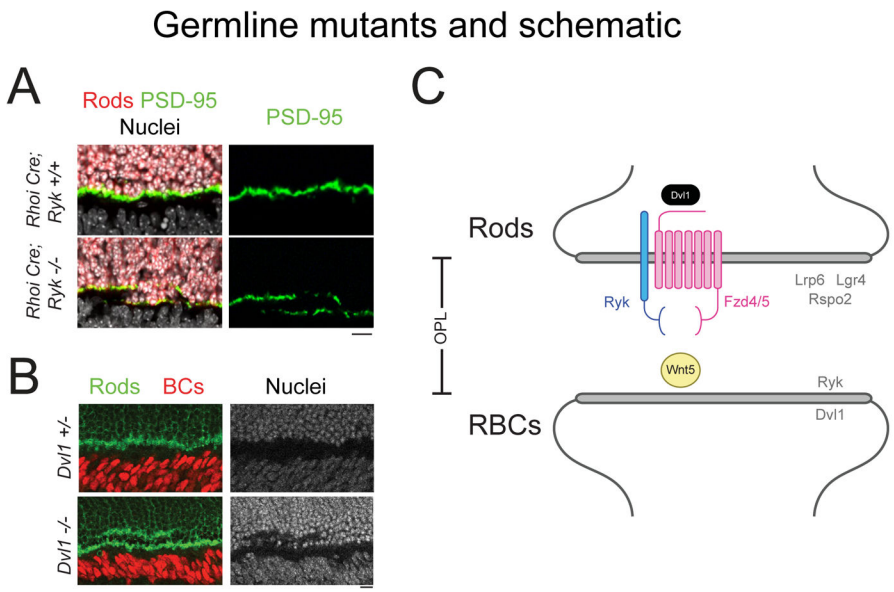

Figure 8. Germline mutants phenocopy CRISPR knockouts

A. Conditional germline knockout of Ryk (Rhoicre; Ai14; *Ryk*$^{flox/flox}$) phenocopies Ryk^{CRISPR}. Markers: OPL, anti-PSD-95 (green), rods: iCre-dependent TdTom (red), Nuclei: DAPI. Scale bar, 10 μm.

B. Germline knockouts of Dvl1 phenocopy Dvl1^{CRISPR}. Markers: OPL, anti-PSD-95; rods, anti-Reep6; Nuclei, TOPRO-3. Scale bar, 10 μm.

C. Summary of Wnt signaling pathway elucidated from experiments.